Modeling the Effect of Climate Change on Suspended Sediment Load and Sediment Resuspension in an Urban River

A thesis submitted by

Shuo Zhao

in partial fulfillment of the requirements for the degree of

Master of Science

in

Civil and Environmental Engineering

Tufts University

February 2014

Advisers: John L. Durant, Steven C. Chapra, and Paul H. Kirshen

ProQuest LLC.
789 East Eisenhower Parkway
P.O. Box 1346
Ann Arbor, MI 48106 - 1346

Abstract

Suspended sediment remains a major challenge for environmental system modeling due to its non-point source feature and complicated transport regime and it has rarely been investigated under the climate change context. This study uses a watershed hydrology and sediment yield model (GWLF) and a hydrodynamic and sediment transport model (WASP) to estimate suspended sediment load and bed material resuspension for the Aberjona River, MA and predict changes in response to variations in future climate. Depending on climate scenario, mean annual suspended load change between -2% to 19% from current level (1950-1999) is found for the Mid-century (2030-2059) and -8% to 18% for the end of the century (2070-2099) while mean annual sediment resuspension is projected to increase by 8% to 52% in the Mid-century and 2% to 89% by the end of the century. Mean monthly suspended load is modeled to change by -87% to 140% for the Mid-century and by -87% to 164% for the end of the century. Change in monthly resuspension varies from -99% to 237% and -100% to 342% for the two scenario periods respectively. The increase of suspended sediment load corresponds to the increase of surface runoff due to more rainfall but higher evapotranspiration caused by warming trend counteracts it. Sediment resuspension is significantly intensified under more frequent occurrence of extreme high flow condition.

Acknowledgements

I am extremely grateful for my thesis committee's strong support for this study. I want to thank my adviser, Dr. John Durant, for providing thoughtful ideas, advices and resources through the entire process with invaluable patience. I would like to acknowledge Dr. Paul Kirshen for putting this study into a wider climate change context and expanding my knowledge on this field. I particularly appreciate Dr. Steven Chapra for introducing me to the power of numerical modeling and my fascination with it. Thanks to Dr. Richard Vogel who have offered precious insight for both this study and my career as have all my thesis committee members.

I would also like to thank Dr. James Limbrunner and my classmates Jeff Walker and Jing Zhu for their knowledge and experiences on numerical model development, GIS application and other technical issues. Thanks to my colleagues and friends in CEE department and WSSS program for making it a wonderful experience for me at Tufts University. Finally, I would like to thank my parents Weijin Zhao and Xianghong Chen for their unconditional love and support as always.

Table of Contents

List of Figures

List of Tables

1 Introduction

Sediment has become one of the leading causes of impairment in rivers and streams in the US. According to EPA National Water Quality Inventory Report, 2002, more than 30% of impaired streams suffer excessive sedimentation which can smother stream beds, suffocate fish eggs and bottom-dwelling organisms, and interfere with drinking water treatment and recreational uses (USEPA, 2007). Watershed surface soil erosion is often thought to be the primary source of suspended sediment in river system. However, during large storm events, bed material resuspension may become another significant mechanism that can generate transient high suspended solids concentration.

Meanwhile, projected changes from both global and regional studies indicated that it is likely that the magnitude and frequency of extreme precipitation events will increase in the 21st century over many areas, especially in northern mid-latitudes in winter (SREX, 2012). This trend will undoubtedly exacerbate both land surface erosion and bed sediment resuspension. And suspended sediment load analysis had rarely been done for a mid-scale urban watershed under climate change context. The goal of this thesis is to develop a mathematical model for the Aberjona River, MA to determine suspended sediment load from various sources and the effect of climate factors on suspended sediment load and sediment resuspension. Then the model will be applied to make sediment yield projections under potential future climatic scenarios.

1.1 Sediment Load Classification

Sediment is a typical nonpoint source (NPS) pollutant. As displayed by Figure 1.1, sediment load, with respect to its source, can be divided into *Bed Material Load*: particles derived from river bed upstream, and *Wash Load*: soil eroded from watershed land surface, either

from natural or anthropogenic sources and entered into waterbody carried by surface runoff. Construction and agriculture can accelerate natural erosion rates, increasing the supply of wash load (Nelson & Booth, 2002).

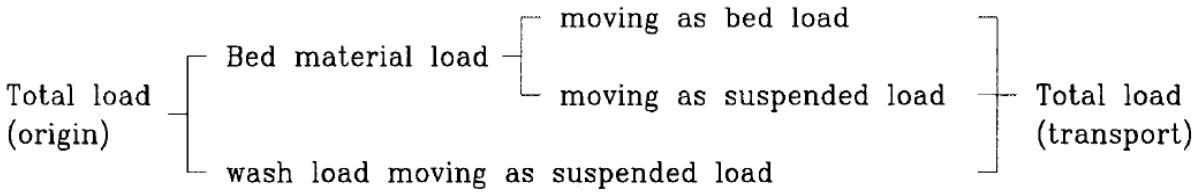

Figure 1.1 Sediment load classification (L. van Rijn 1993).

From a transport perspective, sediment is either moved in almost continuous contact with the riverbed by rolling, sliding, or saltating as bed load or maintained in suspension by turbulence in the flowing water as suspended load (van Rijn, 1993). Sediment bed load is critical to channel morphology and to the operation and maintenance of multiple river-basin projects like hydropower development, flood control and navigation (Einstein, 1950).

Suspended load is comprised of bed material resuspension and wash load. The main environmental impacts of suspended solids include the following: 1) Suspended solids generate turbidity. High turbidity block the light from reaching submerged vegetation, inhibiting their growth and consequently affecting dependent species; 2) Contaminants in river system such as nitrogen, heavy metals and organic toxicants are often hydrophobic, thus tying their fate to suspended solids as their primary carrier (Scott et al., 2010). This study mainly focused on bed material resuspension because during large storm event it may become a significant contributor to suspended load, which could inflict severe damage to river water quality and ecosystem. Moreover, under future climate change scenario, impairment may occur more frequently. Therefore, it is essential to differentiate sediment loads from their various sources and examine their transport regime and water quality impact. To reflect suspended sediment level in the

Aberjona River, the commonly used water quality measurement total suspended solids (TSS) concentration was chosen for this study.

1.2 Sediment Transport

Bed load and suspended load transport mechanism was discussed comprehensively by van Rijn (1984a; 1984b; 1984c), Yang (1996) and Chien et al. (1999). In regard to bed material resuspension, it is necessary to mention a physical concept *initiation of motion* which describes the critical shear stress when the flow condition exceeds it, sediment particles on the river bed start to move. As pointed out by Chien et al. (1999), initiation of motion has gradually been regarded as a stochastic phenomenon since a typical bed surface is comprised of numerous sediment grains of various combinations of sizes, shapes and orientations, and flow fields have fluctuating characteristics. Thus, the forces exerted on particles at different places are different at a specific time point while they are also different at various times for grains at a given place. The movement of bed material is a complex function of flow conditions, sediment supply, and channel characteristics (Einstein, 1950).

Former research on river sediment resuspension is very limited because it is relatively a minor source of suspended load compared to land surface erosion for small river systems like the Aberjona River. Numerous studies either directly measure resuspension using flumes in lab conditions (Roberts et al., (2003); Gust and Morris (1989)) or consider it for other types of water systems like lakes. Bloesch (1994) reviewed current methods to measure lake sediment resuspension including direct quantification (sediment traps, radiotracers etc.) and indirect calculation (mass balance model and statistical analysis) and indicated all those reviewed modeling approaches suffer from various fundamental assumptions which are not fully met in-situ. Gailani et al. (1991) developed a numerical model to simulate transport and fate of

suspended solids in the Lower Fox River and pointed out that resuspension property is significantly affected by particle size variation and cohesion.

1.3 Climate Change across US Northeast

Multiple studies have drawn on state-of-the-art general circulation models (GCMs) to assess the climate change of US Northeast (NECIA, 2006; SREX, 2012).

Temperature rise: According to NECIA (2006), annual temperatures across the Northeast have risen more than 0.83°C while winters have been warming fastest at the rate of 0.72°C per decade since 1970. Under the lower-emissions scenario defined by IPCC Special Report on Emissions Scenarios (SRES) (Nakicenovic et al., 2000), annual temperatures are projected to increase 1.9 to 3.6°C by 2100, and 3.6 to 6.9°C under the higher-emissions scenario. This warming trend will certainly exert notable influence on watershed hydrology in the Northeast. On one hand, higher temperature in winter will make snow melt process earlier and increase flow intensity during high flow period in early spring. On the other, evapotranspiration will be exacerbated and therefore intensify and expand low flow period in summer. These changes on hydrology will affect sediment yield and transport capacity seasonally and periodically.

Extreme precipitation and storms: Rainfall is expected to become more intense while the frequency of extreme storm events is increasing across the US Northeast (NECIA, 2006). Based on projections from NECIA (2006), the average amount of rain that falls on any given rainy day in the Northeast will increase 8% by mid-century, and 10 to 15% by the end of the century. Meanwhile, the number of extreme storm events is also projected to go up by 8% by mid-century, and 12 to 13% by the end of the century. According to SREX (2012), a 1-in-20 year annual maximum 24-hour precipitation amount is projected to become a 1-in-5 to 1-in-10 year event by the end of the 21st century in the Northeast under a range of SRES climate scenarios.

This tendency will intensify watershed soil erosion and cause extreme flow conditions more frequently which can directly affect bed material resuspension.

Climate change effect on river sediment yield and transport had been discussed by literature for relatively large watersheds. However, the results indicated high variability, uncertainty and site specification. Asselman et al. (2003) provided possible impacts of changes in land use and climate on soil erosion, sediment transport, and deposition in the River Rhine using a geographical information system (GIS) based model and found that although erosion will increase 12% averagely over the entire basin, sediment loads were modeled to decrease by 13% in the delta area due to inefficient sediment delivery. The limitation of the understanding of sediment delivery could generate large model uncertainty.

Lu et al. (2013) provided a guideline for evaluating the responses of sediment loads to climate change in similar climate zones based on a preliminary study of eight large Chinese rivers and concluded that precipitation change coupled with rising temperatures has played a significant role in influencing the sediment delivery dynamics over the past decades while human activities such as land cover change and reservoir construction are still the predominant forces. Their results indicated that every 1% change in precipitation has resulted in a 1.3% change in water discharge and a 2% change in sediment loads. In addition, every 1% change in water discharge caused by precipitation has led to a 1.6% change in sediment loads, but the same percentage of water discharge change caused largely by humans would only result in a 0.9% change in sediment loads.

Hancock (2012) investigated the effect of different rainfall patterns on erosion and resultant water quality in a small catchment in Australia using a numerical model (CAESAR) under different rainfall scenarios over a synthetic 1000 year period. The model results revealed

that increased rainfall amount and intensity increased sediment transport rates but the predicted sediment concentration was variable. The more frequent appearance of high rainfall increases sediment load but average concentration may reduce as a result of the increased discharge.

Thodsen et al. (2008) reported that seasonal changes in suspended sediment transport were found between -26% and +68% between the control and the climate change scenario periods for two rivers in Denmark based on results by HIRHAM regional climate model.

Gomez et al. (2009) used a one-dimensional sediment transport model (TUGS) and a climate-driven hydrological model (HydroTrend) to predict changes to the sediment transport regime of the Waipaoa River in response to climate variation and predicted a 75% loss of the river's flood control capacity due to bed level rising.

2 Site Description

2.1 Study Area

The Aberjona River flows 14.5 kilometers from its headwaters in Reading, MA to the Upper Mystic Lake. The watershed is comprised of seven municipalities and covers a drainage area of 6330 hectares. It is heavily urbanized (more than 70% of the watershed area) and impacted by human activities (Figure 2.1 & Figure 2.2).

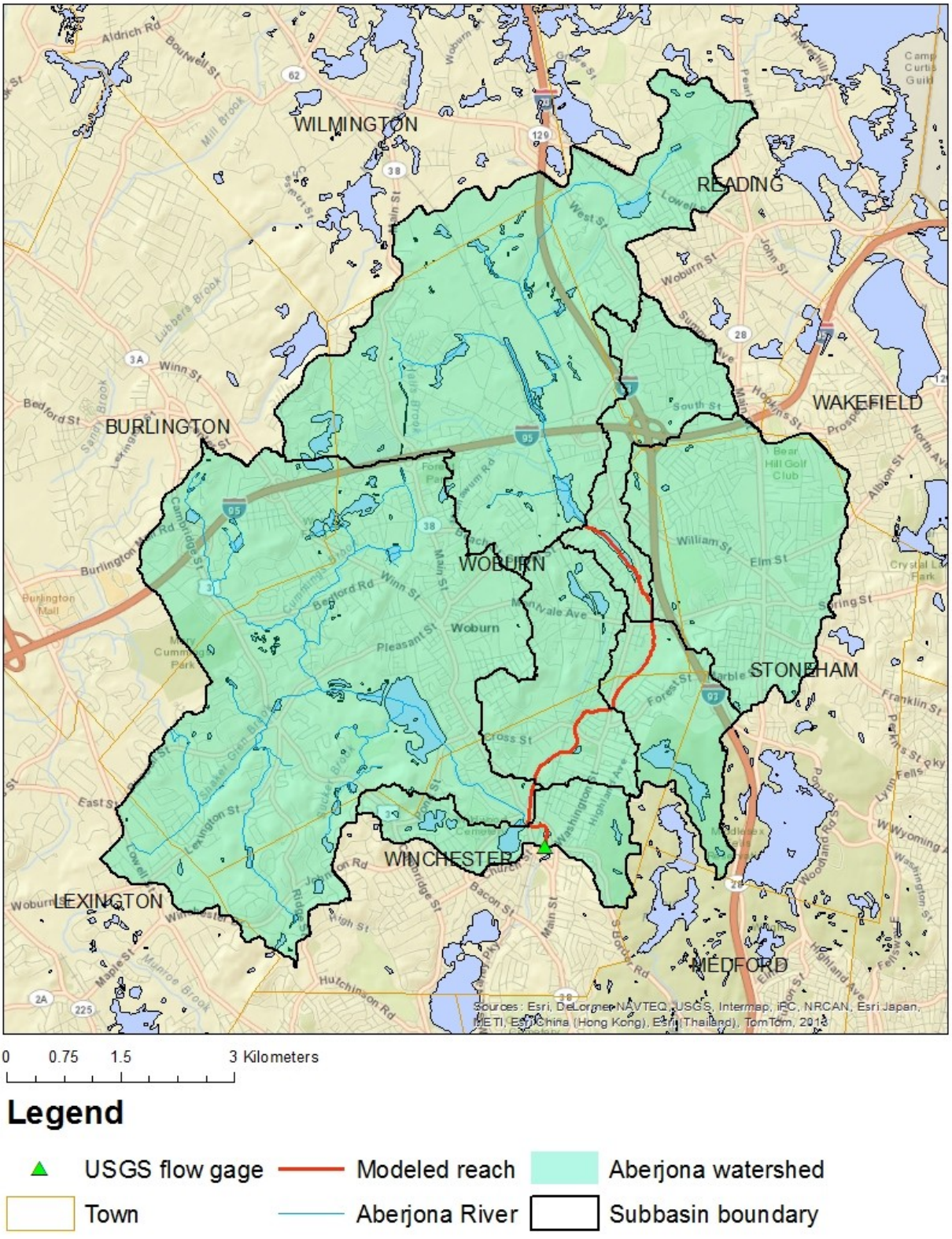

Figure 2.1 Aberjona River watershed (Watershed boundary source: USGS).

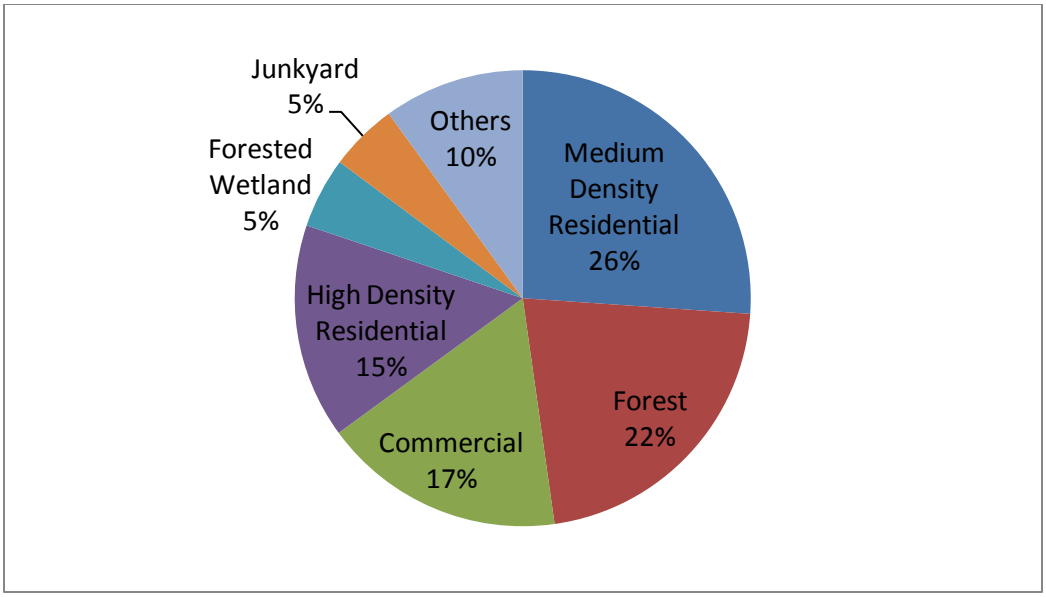

Figure 2.2 Aberjona watershed land use distribution (Source: MassGIS).

2.2 Data Sources

Table 2.1 Available data used for this study.

Data	Description	Source	Period
Streamflow	Continuous daily data	USGS station Aberjona River at Winchester, MA (01102500)	January, 1998 – January, 2004
TSS	Instantaneous concentrations, discontinuous data	National Water-Quality Assessment Program (NAWQA)	October 1998 – September, 2004
		Mystic River Watershed Association (MyRWA)	July, 2000 – December, 2004
Weather	Mean daily precipitation and temperature	NCDC station at Reading, MA (196783)	January, 1998 – January, 2004
Watershed boundary	GIS polygon shapefile	USGS Streamstats	
DEM - Elevation	GIS grid file	MassGIS	2005
Soil	GIS polygon shapefile	NRCS SSURGO	Updated by November, 2012
Land Use	GIS polygon shapefile	MassGIS	2005

As described in Table 2.1, the available sediment data for the Aberjona River are a series of instantaneous and discontinuous in-stream TSS concentrations from 1998 to 2004 (123 data

points). Figure 2.3 displays TSS concentration overtime with the average daily discharge. Figure 2.4 plots TSS concentration versus discharge on a log scale. These observations did capture some high TSS concentration during large flow events, but the relationship between the TSS concentration and flow condition are nonlinear and not clear. Moreover, it's not possible to attribute any high instantaneous concentration observation to certain sediment sources since there is no direct measurement of sediment resuspension from the river bed or stormwater sampling to investigate wash load form watershed erosion during that period.

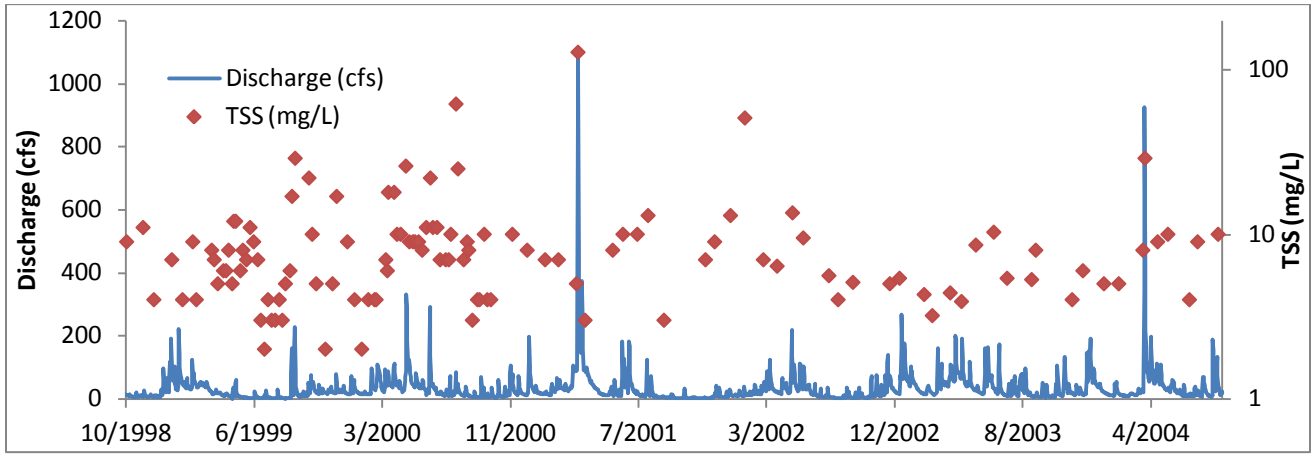

Figure 2.3 Discharge (real space) with TSS concentration (log space) 1998-2004.

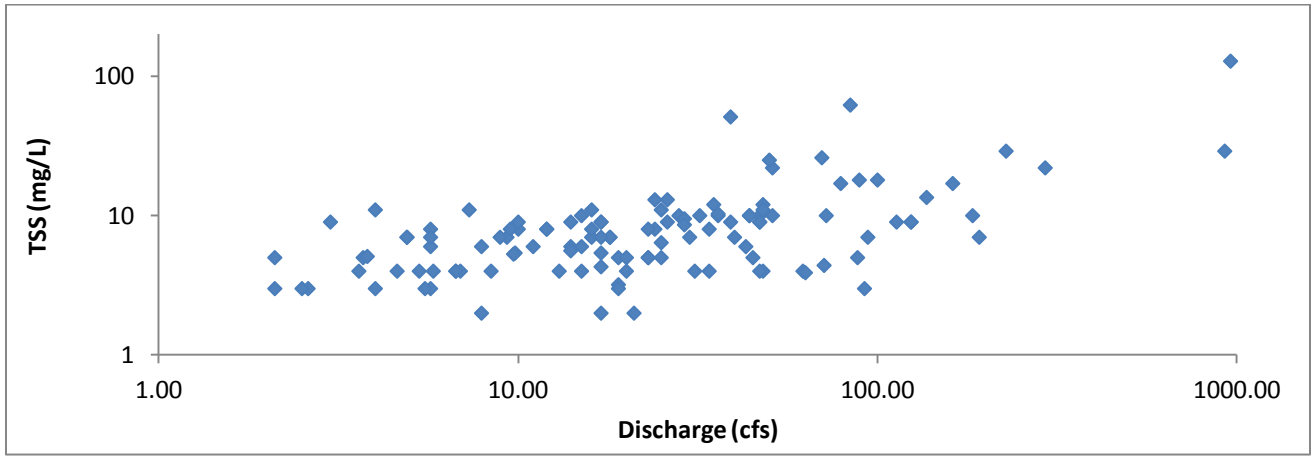

Figure 2.4 TSS concentration versus Discharge (log space) 1998-2004.

3 Methodology

Due to the data limitations described in Chapter 2.2 and the sediment as a non-point source pollutant, distributed model needs to be applied to quantify sediment resuspension. A combination of a watershed model and a hydrodynamic and sediment transport model was used to estimate sediment loads from different sources and simulate sediment transport for the Aberjona River reach which starts from MyRWA sample location ABR049 at Woburn, MA (an outfall of EPA super-fund site Industri-Plex) to USGS gage 01102500 at Winchester, MA (red line in Figure 2.1). The river mainstream was segmented into 5 compartments based on their relatively uniform channel geometry and the watershed was divided into 7 subbasins using GIS (Figure 2.2).

3.1 Watershed Model (GWLF)

Both deterministic and stochastic watershed models can be developed using existing data. However, stochastic watershed models are based on the stationary assumption that future hydrology will not significantly deviate from past hydrology (Barsugli et al., 2012). The current scientific understanding of climate change fundamentally challenges this assumption (Milly et al., 2008). In this study, since climate change factors must be accounted for, a physically-based deterministic watershed model which has the capability to calculate sediment loads from watershed soil erosion needs to be built. Therefore, Generalized Watershed Loading Functions (GWLF) was chosen.

Due to its low data requirements on input and calibration efficiency, GWLF has been widely used in Total Maximum Daily Load (TMDL) development to calculate watershed pollutant loads (Schneiderman et al., 2002; Howarth et al., 1991; Lee et al., 2000). Originally,

GWLF was a deterministic watershed model developed to predict annual and monthly streamflow, soil erosion and sediment yields (Haith et al., 1992).

However, to quantify sediment resuspension, a continuous daily simulation of sediment loads must be conducted. Geographic Information System (GIS) is applied for input data processing and GWLF algorithm was coded in Visual Basic with the modification to execute daily simulation suggested by Tabak (2003). The following section presents the detailed principles of the two main components of this modified GWLF model.

3.1.1 Hydrology Model in GWLF

Streamflow is calculated by sum of watershed runoff from all sources areas and groundwater discharge from a shallow saturated zone. Daily runoff is computed from weather data by the U.S. Soil Conservation Service's Curve Number (CN) method (Ogrosky & Mockus, 1964).

$$Q_{kt} = \frac{(R_t + M_t - 0.2DS_{kt})^2}{R_t + M_t + 0.8DS_{kt}} \quad \textbf{(3-1)}$$

$$M_t = 0.45T_t \,, T_t > 0℃ \quad \textbf{(3-2)}$$

Q_{kt} (cm) is daily runoff from each land use category k. R_t (cm) and M_t (cm) are rainfall and snowmelt on day t respectively. DS_{kt} (cm) is detention parameter based on curve number

$$DS_{kt} = \frac{2540}{CN_{kt}} - 25.4 \quad \textbf{(3-3)}$$

Curve number for each land use CN_{kt} is designated by the user and then calculated as a function of 5-day antecedent moisture conditions A_t (cm) (Haith et al., 1992):

$$A_t = \sum_{n=t-5}^{t-1} (R_n + M_n) \quad \textbf{(3-4)}$$

Groundwater discharge is described by a lumped parameter model (Figure 3.1). Soil moisture for the unsaturated S_t and shallow saturated zones U_t is defined by:

$$U_{t+1} = U_t + R_t + M_t - Q_t - E_t - PC_t \quad \textbf{(3-5)}$$

$$S_{t+1} = S_t - G_t - D_t + PC_t \quad \textbf{(3-6)}$$

E_t, PC_t, G_t and D_t are evapotranspiration, percolation into the shallow saturated zone, groundwater discharge and groundwater seepage to the deep saturated zone (cm).

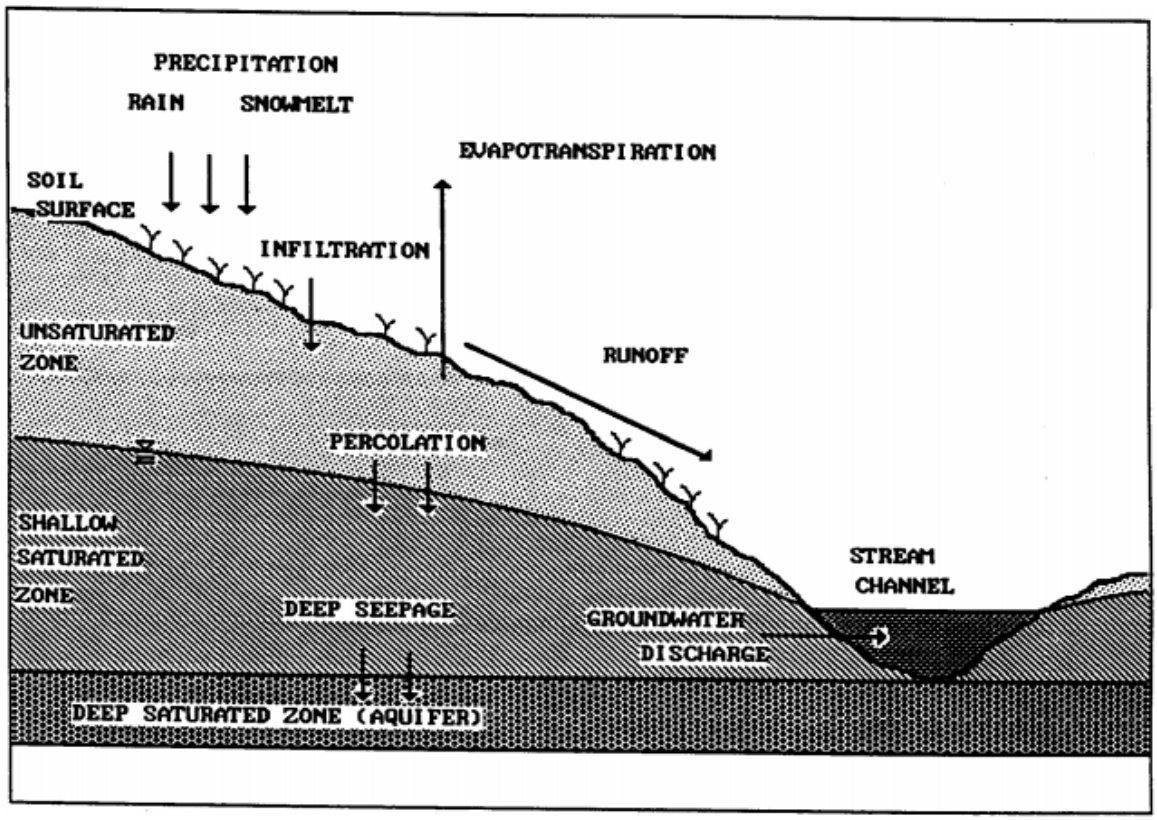

Figure 3.1 Lumped parameter model for groundwater discharge (Haith et al., 1992).

Percolation PC_t (cm) occurs when available water capacity of the unsaturated zone U^* (cm) is exceeded:

$$PC_t = Max(0;\ U_t + R_t + M_t - Q_t - E_t - U^*) \quad \textbf{(3-7)}$$

Evapotranspiration E_t (cm) is calculated limited by available moisture in the unsaturated zone

$$E_t = Min(CV_t PE_t;\ U_t + R_t + M_t - Q_t) \quad \textbf{(3-8)}$$

Where PE_t is potential evapotranspiration (cm) as given by (Hamon, 1961) and CV_t is a model parameter cover coefficient.

$$PE_t = \frac{0.021 H_t^2 e_t}{T_t + 273} \quad \textbf{(3-9)}$$

In which T_t is the mean daily temperature (°C) on day t, H_t is the number of daylight hours per day on day t, e_t is the saturated water vapor pressure (millibar) on day t.

Groundwater discharge G_t and deep seepage D_t is defined by:

$$G_t = rS_t \quad \textbf{(3-10)}$$

$$D_t = sS_t \quad \textbf{(3-11)}$$

Where r and s are groundwater recession and seepage coefficients.

3.1.2 Sediment Yield Model in GWLF

3.1.2.1 Rural Sediment Yield

Rural sediment yield is estimated based on soil erosion and sediment transport mechanism. Universal Soil Loss Equation (USLE) (Wischmeier & Smith, 1978) is employed in GWLF to compute soil erosion:

$$X_{kt} = 0.132 RE_t K_k (LS)_k C_k P_k A R_k \quad \textbf{(3-12)}$$

In which K_k, $(LS)_k$, C_k, P_k and AR_k are values for soil erodibility, topographic, cover and management factors, supporting practice factors and area for each land use. The rainfall erosivity is estimated by:

$$RE_t = 64.6 a_t R_t^{1.81} \quad \textbf{(3-13)}$$

Where a_t is a coefficient that varies with season and geographical location. For southern New England, typical a_t value is 0.11 for October to March and 0.22 for April to September (Selker et al., 1990).

To calculate sediment yield, a daily transport factor TR_j is defined as $TR_t = Q_t^{5/3}$. And daily transport capacity B_j is determined by:

$$B_t = \sum_{t=j}^{D} TR_t \quad \textbf{(3-14)}$$

Where j is the Julian day of the model year and D is the number of days per year. The model assumes that transport capacity decreases as each day passes during a model year. Finally, daily rural sediment yield Y_t is

$$Y_t = DR * TR_t \sum_{j=1}^{t} \frac{X_j}{B_j} \quad \textbf{(3-15)}$$

In which DR is sediment delivery ratio designated by the user.

3.1.2.2 Urban Sediment Build-up/Wash-off Function

To calculate sediment loads from urban impervious area, the enhanced GWLF model includes a build-up/wash-off function proposed by (Amy et al., 1974) and (Sartor & Boyd, 1972) which follows a process that eroded soil accumulates on watershed land surfaces between storm

events and then washed off when surface runoff occurs. The daily accumulated sediment load is calculated by an exponential accumulation function:

$$N_{k,t+1} = N_{kt}e^{-0.12} + [\frac{n_k}{0.12}(1 - e^{-0.12})] \quad \textbf{(3-16)}$$

Where N_{kt} is the sediment accumulation at the beginning of day t, n_k is accumulation rate constant. Equation 3-15 is derived by assuming that $N_k(t)$ reaches 90% of $N_{k,max}$ in 20 days (Haith et al., 1992).

Sediment loads carried by runoff is:

$$W_{kt} = w_{kt}[N_{kt}e^{-0.12} + \frac{n_k}{0.12}(1 - e^{-0.12})] \quad \textbf{(3-17)}$$

Where $w_{kt} = 1\text{-}e^{-1.81Q_{kt}}$ is the first-order wash off function based on the assumption that 0.5 inches of runoff will wash off 90% of accumulated sediment (Amy et al., 1974).

Total daily sediment yield is then defined as:

$$Y_t = DR * TR_t \sum_{J=1}^{T} \frac{X_j + W_j}{B_j} \quad \textbf{(3-18)}$$

3.2 Hydrodynamic and Sediment Transport Model (WASP7)

A mechanistic transport model Water Quality Analysis Simulation Program (WASP7) was applied in this study to simulate hydrodynamic and sediment transport in the Aberjona River. This model had widely been used for eutrophication, toxicant transport and multiple pollutants TMDL analysis (Kim et al., 2007; Zhang & Rao, 2012; Yenilmez & Aksoy, 2013; Meric et al., 2013).

3.2.1 Hydrodynamic Module in WASP

There is a spectrum of models that are available to simulate dynamic water movement for streams which are all based on the St. Venant equations (Chapra, 2008):

Continuity equation (mass balance):

$$\frac{\partial Q}{\partial x} + \frac{\partial A}{\partial t} = 0 \quad \textbf{(3-19)}$$

Momentum equation (momentum balance):

$$\frac{1}{A}\frac{\partial Q}{\partial t} + \frac{1}{A}\frac{\partial}{\partial x}\left(\frac{Q^2}{A}\right) + g\frac{\partial y}{\partial x} - g\left(S_0 - S_f\right) = 0 \quad \textbf{(3-20)}$$

WASP executes flow routing through a branching stream network based on kinematic wave equation, a solution of St. Venant equations that only considers the effects of gravity and friction (Ambrose, 2009):

$$g\left(S_0 - S_f\right) = 0 \quad \textbf{(3-21)}$$

where g is acceleration of gravity, S_0 is the bottom slope and S_f is the friction slope. Bringing in Manning's equation of flow velocity:

$$U = \frac{1}{n}R^{2/3}S_0^{1/2} \quad \textbf{(3-22)}$$

in which n is Manning's roughness, R is hydraulic radius which is equivalent to the cross-sectional area A divided by wetted perimeter P.

Substituting these into Manning's equation and rearranging terms gives:

$$Q = UA = \frac{1}{n}\frac{A^{5/3}}{P^{2/3}}S_0^{1/2} \quad \textbf{(3-23)}$$

For rectangular channel which width is considerably larger than water depth, P can be expressed as channel width B, Eq. 3-22 can be solved for

$$A = \alpha Q^{\beta} \tag{3-24}$$

where β = 3/5 and

$$\alpha = \left(\frac{nB^{2/3}}{\sqrt{S_0}}\right)^{3/5} \tag{3-25}$$

Incorporating Eq. 3-23 into Eq. 3-18 gives the kinematic wave differential equation:

$$\frac{\partial Q}{\partial x} + \alpha\beta Q^{\beta-1}\frac{\partial Q}{\partial t} = 0 \tag{3-26}$$

WASP contains Euler and Runge-Kutta method options to generate numerical solution for Eq. 3-25.

3.2.2 Sediment Transport Module in WASP

Sediment transport module in WASP assumes there is a constant volume sediment layer corresponding to each free flowing segment (Figure 3.2).

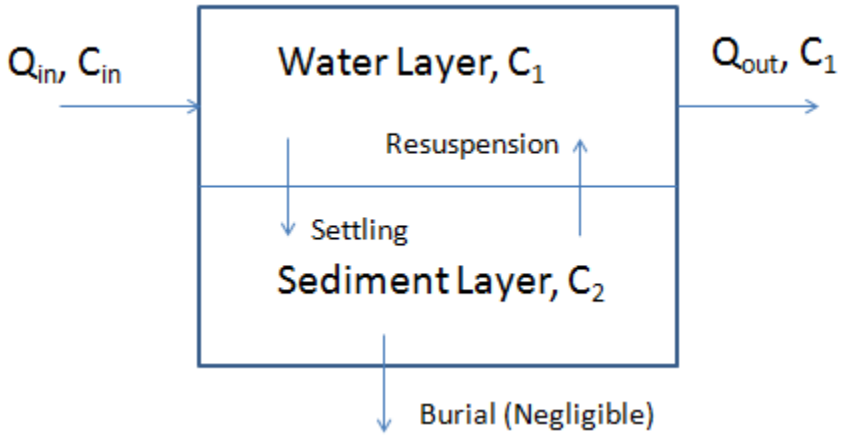

Figure 3.2 Sediment transport module in WASP.

So the TSS concentration in each benthic compartment and water column can be calculated by solving the simple one-dimensional solid mass balance.

$$V_1 \frac{dc_1}{dt} = Q_{in}c_{in} - Q_{out}c_1 - v_s A_s c_1 + v_r A_s c_2 \quad \textbf{(3-27)}$$

$$V_2 \frac{dc_2}{dt} = v_s A_s c_1 - v_r A_s c_2 - v_b A_s c_2 \quad \textbf{(3-28)}$$

V_1, c_1, V_2 and c_2 are the segment volume and TSS concentration of water layer and its corresponding sediment layer respectively. Q_{in}, c_{in} are streamflow and TSS concentration from last river reach. v_s, v_b and v_r are sediment settling, burial and resuspension velocity respectively. A_s is the area of sediment-water interface. Streamflow into and out of each segment is obtained by the flow routing process in WASP. However, since WASP includes no process descriptions for solids transport, settling and resuspension velocity must be designated by the user.

3.3 Model Combination

WASP requires streamflow and sediment loads data from each subbasin as input to execute its flow routing and transport simulation. As stated in Chapter 2.2, there is no measurement that has been conducted to obtain such data. Therefore, the output of GWLF was linked to WASP as input to combine these two models. Figure 3.3 displayed the integrated model scheme.

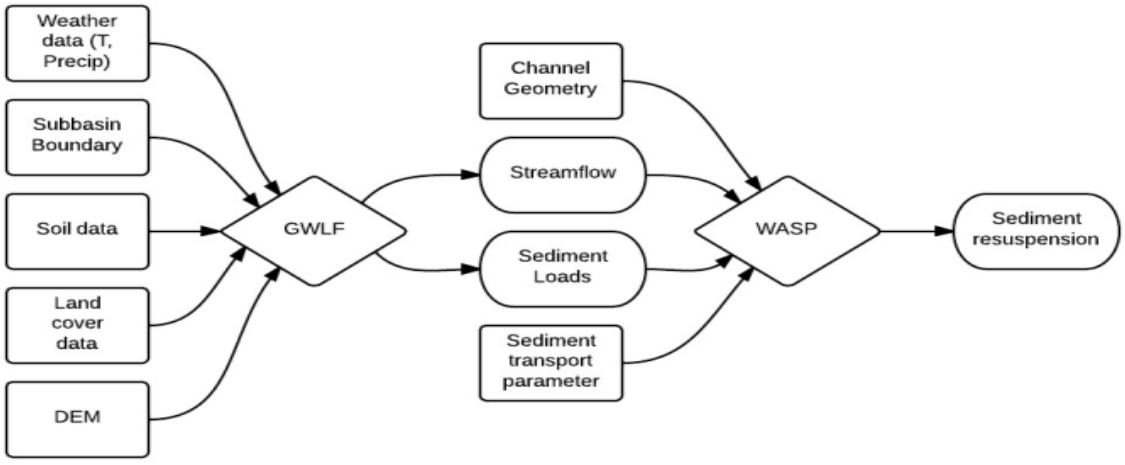

Figure 3.3 Combination of GWLF & WASP.

4 Model Calibration and Validation

Consider existing TSS data, October, 1998 – September, 2001 is designated as calibration period, while October, 2001 – September 2004 as validation period.

4.1 GWLF Calibration and Validation

4.1.1 Hydrology Model Calibration

GIS was widely applied to generate input for GWLF calibration. To calculate curve numbers (CN), GIS land use and urban impervious cover data from MassGIS were first combined with Hydro Soil Group data from soil survey geographic database SSURGO established by Natural Resources Conservation Service (NRCS). Then curve numbers were assigned following the guidance of USDA Technical Release 55 (NRCS, 1986) to each grid within the watershed boundary. Also, SSURGO provided available water capacity (U*) data and area-weighted U* was calculated for the entire watershed.

Daily precipitation and average temperatures from National Climate Data Center (NCDC) were imported into GWLF. The parameters remained to be determined in GWLF hydrology model were cover coefficients CV, deep seepage constant s and groundwater recession constant r. Haith et al. (1992) pointed that no universally accepted techniques are available for estimating deep seepage rate constant and the most conservative approach is to assume s equals to 0. Also for recession constant r, Haith et al. (1992) reported typical values nationwide range from 0.01 to 0.2 and 0.06 is common in the US northeast. In this study, s was set to 0 then CV and r were searched by minimizing the sum of root mean square errors (RMSE) between modeled discharge and observations from USGS gage using Solver in Excel.

Coefficient of determination (R^2) and Nash-Sutcliffe efficiency (NSE) were used as measure of goodness of fit. NSE is defined as (Nash & Sutcliffe, 1970):

$$NSE = 1 - \frac{\sum_{i=1}^{N}((q_m(i) - q_o(i))^2}{\sum_{i=1}^{N}(q_0(i) - \bar{q}_o)^2} \quad \textbf{(4-1)}$$

in which q_m is estimated discharge, q_o is observed discharge and $\bar{q}_o$ is the average observed discharge over the calibration period.

4.1.2 Improved hydrology model

In initial calibration runs, R^2 and NSE were no larger than 0.55 and 0.5 respectively. It was found that the model tended to overestimate surface runoff during large storm events while underestimating it during small events. Meanwhile, mean annual streamflow was significantly larger than observation. Therefore, improvements were made mainly based on (Tabak, 2003) and summarized as follow:

1) *Cover Coefficient*. In original GWLF model, CV ranges from zero to one based on the theory that the maximum value of ET is the calculated PET. In this study, even when CV was set to unity, mean annual streamflow was still tremendously higher than observation which indicated that Hamon method of PET may underestimate the potential evapotranspiration in the Aberjona watershed. As proved by Tabak (2003), when CV was greater than one, the performance of the model enhanced significantly.

2) *Snowmelt/Accumulation Temperatures.* GWLF uses zero degrees Celsius as critical temperature for both snowmelt and accumulation. However, since the model use averaged daily temperature as input, this assumption may not hold for cases when there was a large temperature difference between day and night. For a warm day with a cold night which have an average temperature above zero degree, precipitation at night may still stick which contradicts the

model's assumption that snowmelt triggers when average T>0 ℃ (Eq. 3-2). Thus the improved model included different temperatures for snowmelt and snow accumulation.

3) *Runoff Curve Number Equation*. Woodward et al. (2003) reported a new initial abstraction ratio 0.05 which gave a better fit to event rainfall-runoff data from several hundred plots:

$$Q_{kt} = \frac{(R_t + M_t - 0.05DS_{kt})^2}{R_t + M_t + 0.95DS_{kt}} \quad \textbf{(4-2)}$$

$$CN_{0.05} = \frac{100}{1.879\left(\frac{100}{CN_{0.20}} - 1\right)^{1.15} + 1} \quad \textbf{(4-3)}$$

where $CN_{0.20}$ is the commonly used curve number in the original GWLF model and $CN_{0.05}$ is the modified curve number under new initial abstraction ratio.

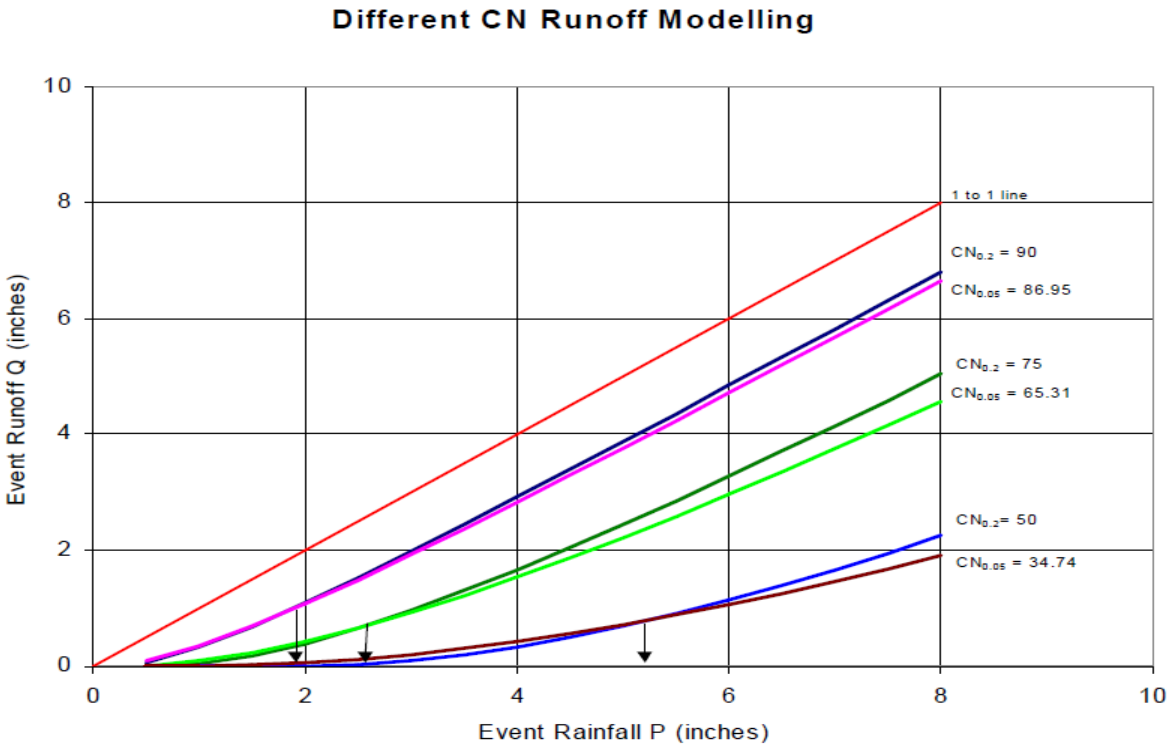

Figure 4.1 Runoff comparison for three conjugate CN pairs (Woodward et al., 2003).

Figure 4.1 indicated that for a specific CN, Woodward's equation provided higher runoff results during lower rainfall than the widely used equation while lower runoff during higher

rainfalls. This exactly fixed the runoff estimation problem described in initial model runs. So the model codes were modified to apply this new curve number and runoff equation.

4.1.3 Sediment Yield Model Calibration

For rural sediment yields, area-weighted soil erodibility factor K and length-slope factor LS in USLE were calculated using GIS Spatial Analyst based on SSURGO soil data and digital elevation model (DEM) data from MassGIS. The cover coefficient C and management practice P factors were assigned according to GWLF 2.0 User's Manual (Haith et al., 1992).

For urban area, Table 4.1 displayed the soil build-up rates estimated with guidance of (Kuo et al., 1988).

Table 4.1 Soil erosion rate in the Aberjona watershed.

Urban Land Use	Soil Build-up Rate (kg/ha/d)
Low Density Mixed	1.26
Medium Density Mixed	3.86
High Density Mixed	3.12
Low Density Residential	1.69
Medium Density Residential	2.99
High Density Residential	3.03

Since eroded soil from watershed land surface flushed by surface runoff may be deposited or trapped by vegetative cover or Best Management Practice (BMP) infrastructure before reaching water bodies, GWLF contains a sediment delivery ratio DR to represent the proportion of eroded soil which finally reaches the waterbody to become wash load. An empirical equation described in (Vanoni, 1975) was used in this study to calculate DR:

$$DR = 0.451(A^{-0.298}) \quad \textbf{(4-4)}$$

in which A is the area of the watershed in square kilometers.

4.1.4 Improved Sediment Yield Model

Original GWLF can only calculate sediment wash load. So when there was no runoff, the model assumed no sediment transported into waterbody on that day. This obviously violated the truth since the TSS concentration data from NAWQA showed that a sediment load did occurred on non-event days. This simply cannot be attributed only to sediment resuspension since the phenomenon is insignificant during low flow period. Tabak (2003) compared a power relationship and a linear relationship based on the same NAWQA data used in this study and determined that a constant non-event baseflow concentration (6.0 mg/L) was sufficient to improve the model. Therefore, a baseflow concentration was programmed into GWLF. The total suspended sediment load became:

$$Suspended\ Load = Wash\ Load + Baseflow\ Load + Resuspension \quad \textbf{(4-5)}$$

$$Baseflow\ Load = Baseflow\ concentration * Discharge \quad \textbf{(4-6)}$$

It should be noted that this baseflow load represents suspended sediment from multiple sources which the integrated model in this study cannot determined mechanistically. These sources include: streambank erosion and bed material resuspension from the Aberjona River's tributaries.

4.2 WASP Calibration and Validation

The improved GWLF model was executed repeatedly for each subbasin to obtain streamflow and sediment loads. These results were linked to WASP as input files. Channel geometry of each river segment was determined from GIS map and personal experience (Table 4.2).

Table 4.2 WASP segment geometry.

WASP Segment Number	Channel Length (m)	Channel Width (m)	Channel Slope	Manning's Roughness
1	1662	5.2	0.0012	0.04
2	1413	5	0.0021	0.04
3	1653	10	0.0006	0.04
4	592	12	0.0017	0.04
5	510	16	0.0020	0.04

Due to the lack of grain size distribution and particle characters from available TSS data, it is not possible to derive the sediment transport properties theoretically in this case. To simplify transport simulation, the study assumed the median sediment diameter in the river is 0.01 mm and fine sediment is not affected by cohesion.

Settling velocity v_s was calculated as the product of the Stokes velocity V_s (m/s) and the probability of deposition:

$$V_s = \frac{1}{18}\frac{\rho_p - \rho_w}{\mu} g {d_p}^2 \quad \textbf{(4-7)}$$

$$v_s = V_s \alpha_D \quad \textbf{(4-8)}$$

where μ is absolute viscosity of water, 0.01 poise at 20 °C; ρ_p is density of the solid which assumed to be 2650 kg/m^3; ρ_w is density of water, 1000 kg/m^3; g is acceleration of gravity, 9.81 m/s^2; d_p = particle diameter, 1.0*10^{-5} m; α_D = the probability of deposition upon contact with the bed (model parameter).

A wide variety of empirical relations to determine resuspension velocity or entrainment rate of noncohesive bed sediment into suspension can be found in the literature (Einstein, 1950; Engelund & Fredsoe, 1976; Smith & McLean, 1977). As pointed out by (Garcia & Parker, 1991), most of entrainment rate are in the form of:

$$E \sim \tau_b^P \sim u_*^{2P} \quad \textbf{(4-9)}$$

where τ_b is bed shear stress due to skin friction; u_* is the associated shear velocity; *P* takes values between 1 and 15, depending on which formulation is considered. They compared seven such relations against a common set of experimental data for which direct measurements of near-bed concentration are available. The relations put forward by (van Rijn, 1984b) were found to perform best. Thus, van Rijn's equation was applied to calculate resuspension velocity v_r:

$$E = 0.015 \frac{D}{k_s} \left(\frac{\tau_s^*}{\tau_c^*} - 1 \right)^{1.5} Re_p^{-0.2} \quad \textbf{(4-10)}$$

$$v_r = E/(1-\phi)\rho_b \quad \textbf{(4-11)}$$

where k_s is roughness height which is set to 1% of water depth, D is particle size, ρ_b is equilibrium bed surface layer concentration, ϕ is porosity of sediment which is assumed to be 0.9 and Re_p is particle Reynolds number defined as:

$$Re_p = \frac{\sqrt{RgD}D}{\upsilon} = \frac{\sqrt{\left(\frac{\rho_p - \rho_w}{\rho_w}\right) gD}D}{\upsilon} \quad \textbf{(4-12)}$$

in which υ is the kinematic viscosity of water, R is submerged specific gravity of sediment. Shields number τ_s^* in Eq. 4-10 is defined as:

$$\tau_s^* = \frac{\tau_b}{\rho_w RgD} \quad \textbf{(4-13)}$$

while bed-shear stress τ_b was calculated by:

$$\tau_b = \frac{\rho_w f u^2}{8} \quad \textbf{(4-14)}$$

$$f = \frac{0.24}{log^2(\frac{12H}{k_s})} \quad \textbf{(4-15)}$$

in which H is water depth and u is water velocity. The critical Shields number τ_c^* in Eq. 4-9 was evaluated with the (Brownlie, 1981) fit to the Shields curve:

$$\tau_c^* = 0.22Re_p^{-0.6} + 0.06 * 10^{(-7.7Re_p^{-0.6})} \quad \textbf{(4-16)}$$

The suspended load from bed material resuspension was then calculated by:

$$Load_{resuspension} = v_r * (1-\phi)\rho_b * A_s \quad \textbf{(4-17)}$$

where v_r is resuspension velocity and A_s is the area of water and sediment layer interface.

The entire model execution followed the procedure: 1) Execute WASP flow module; 2) Read temporarily water depth from step 1 results to compute bed shear stress and resuspension velocity; 3) input sediment settling and resuspension velocity into WASP and perform sediment transport simulation.

4.2.1 WASP Improvement

TSS results from earlier model tests seemed not able to capture most high TSS concentration observed during large storm event. A possible explanation is the settling velocity might be too high so the proportion of sediment which deposited was overestimated. However, the problem remained even when settling velocity was set to zero arbitrarily. Another reason is the incompatibility between original GWLF results and the requirement of WASP input.

WASP requires user to input sediment loads as a loading rate [M/T] at a specific moment in the simulation period. Then it obtains sediment loads by linear interpolation for each time step during execution. However, GWLF only provides sediment yields [M] at a daily time step. Therefore, by directly importing the results from GWLF, sediment loads will be evenly distributed within a day during WASP simulation. But this obviously cannot represent the transport manner of sediment wash load during storms. As suggested by (Alley, 1981), wash-off

process followed a "first flush" rule where pollutants are more highly concentrated in runoff occurring at the beginning of a storm than later. Since only daily precipitation data is available, there is no way to determine when exactly the wash-off process began and its duration within a day. Thus in this study, wash-off was assumed to start in the middle of a day and last for an hour. Sediment loads from GWLF were modified in this manner and linked to WASP.

4.3 GWLF/WASP integrated model results

Figure 4.2 and 4.3 showed the results of GWLF/WASP flow calculation and confirmation. Table 4.3 provided the goodness-of-fit results of the integrated model obtained by comparing daily mean values with data. Both R^2 and NSE values for flow and TSS concentration calibration were larger than 0.7 which indicated that the GWLF/WASP model performed well with satisfactory accuracy. For validation period, the model also proved its prediction capacity by generating R^2 and NSE values lager than 0.6.

Table 4.3 GWLF/WASP model efficiency.

Result	Year	R^2	NSE
Flow	Calibration 1998-2001	0.775	0.738
	Validation 2001-2004	0.699	0.654
TSS concentration	Calibration 1998-2001	0.716	
	Validation 2001-2004	0.633	

Figure 4.4 and 4.5 plotted modeled daily mean TSS concentration versus the NAWQA data and it appeared that the modeled TSS concentration for storm peak and non-storm period generally ranged from 100 to 300 mg/L and 1 to 25 mg/L respectively which was consistent with available data. Figure 4.6 and 4.7 plotted the modeled suspended load for calibration and validation period. Figure 4.8 and 4.9 displayed modeled bed material resuspension from the Aberjona mainstream versus daily precipitation data. The results clearly demonstrated the speculation that resuspension increases significantly during large flow events.

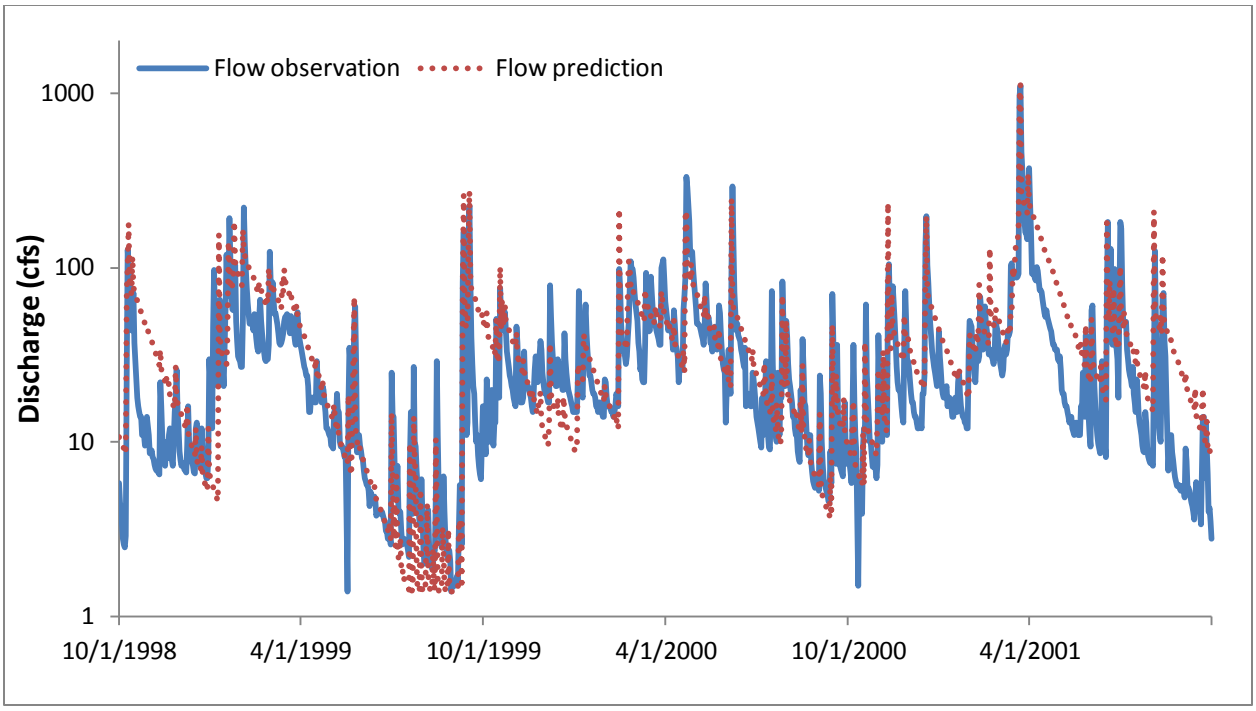

Figure 4.2 GWLF/WASP flow calibration 1998-2001.

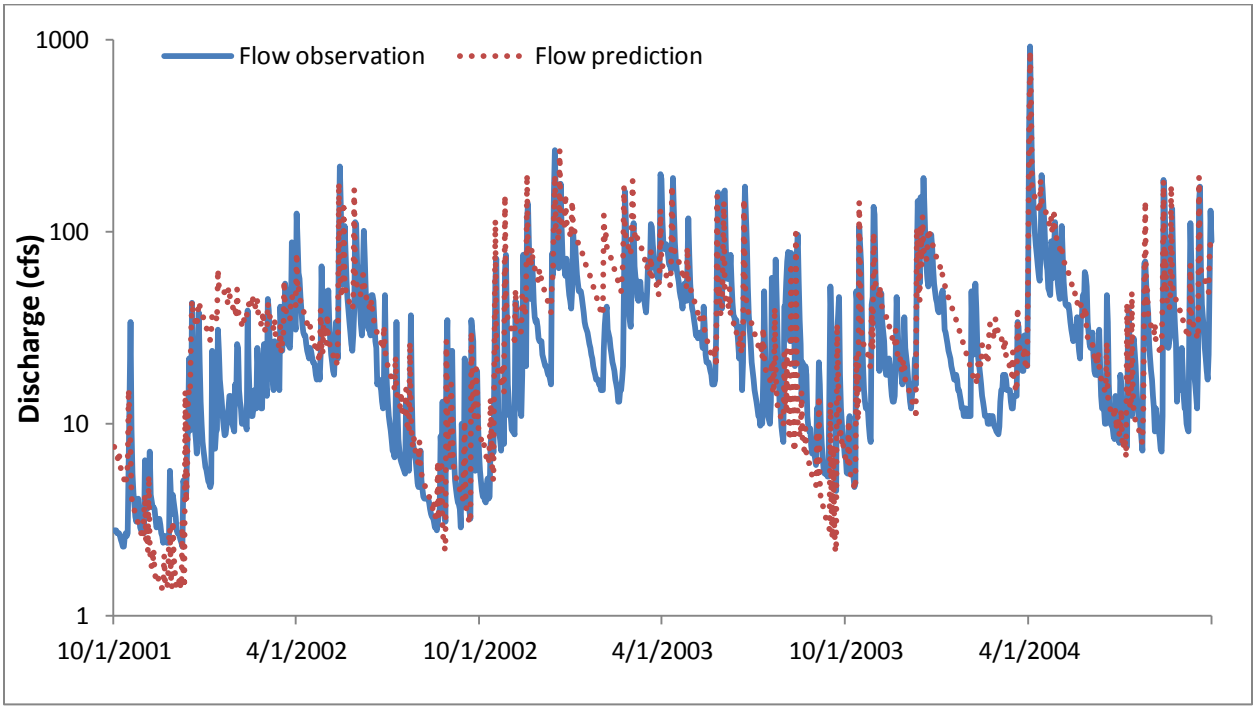

Figure 4.3 GWLF/WASP flow validation 2001-2004.

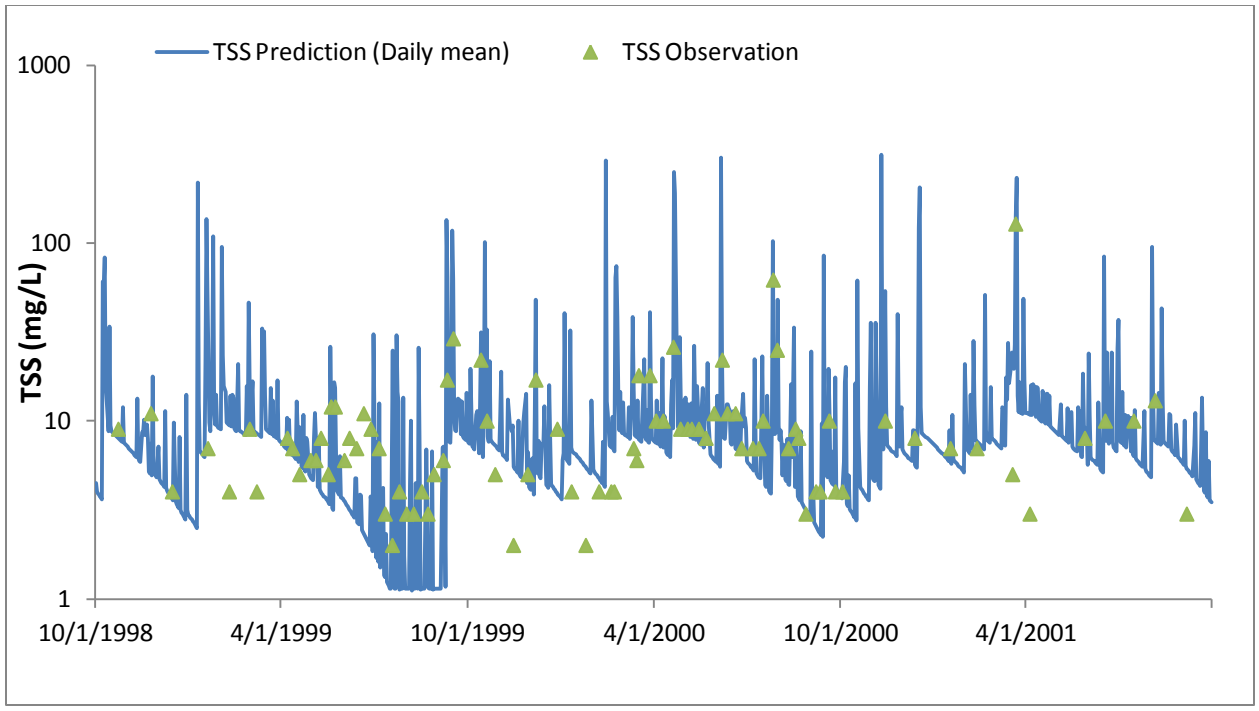

Figure 4.4 TSS concentration calibration (daily mean vs. observation) 1998-2001.

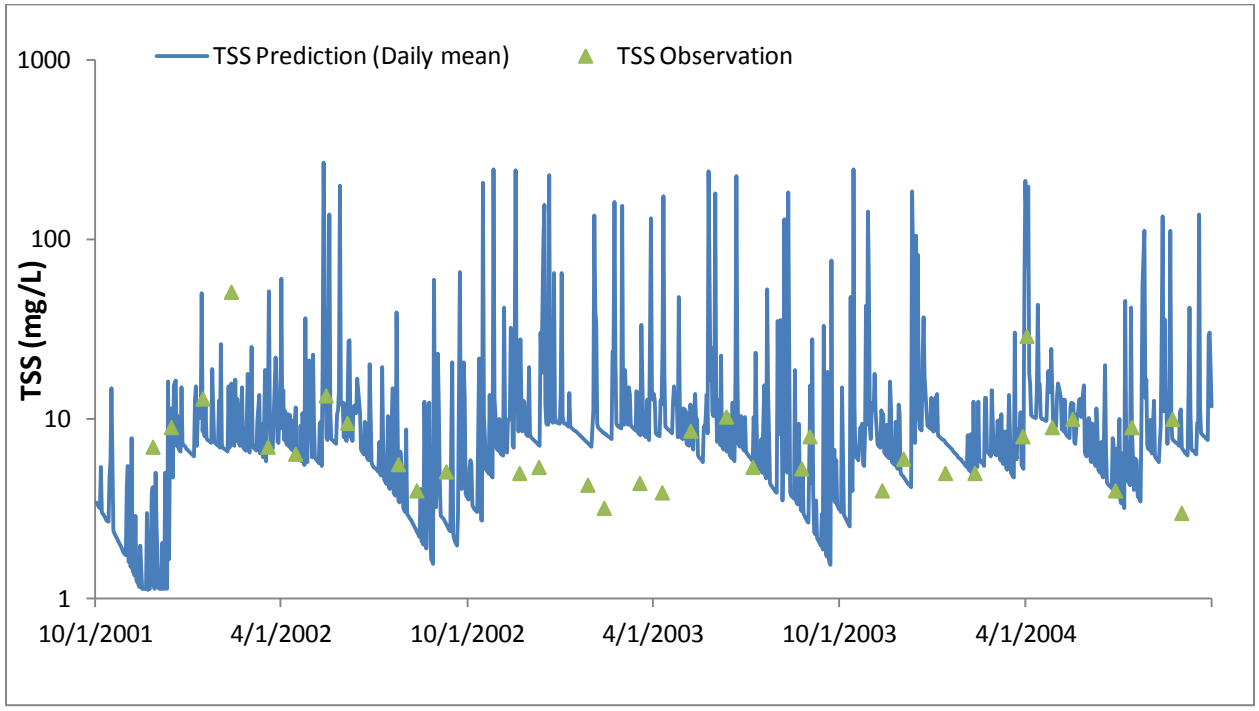

Figure 4.5 TSS concentration validation (daily mean vs. observation) 2001-2004.

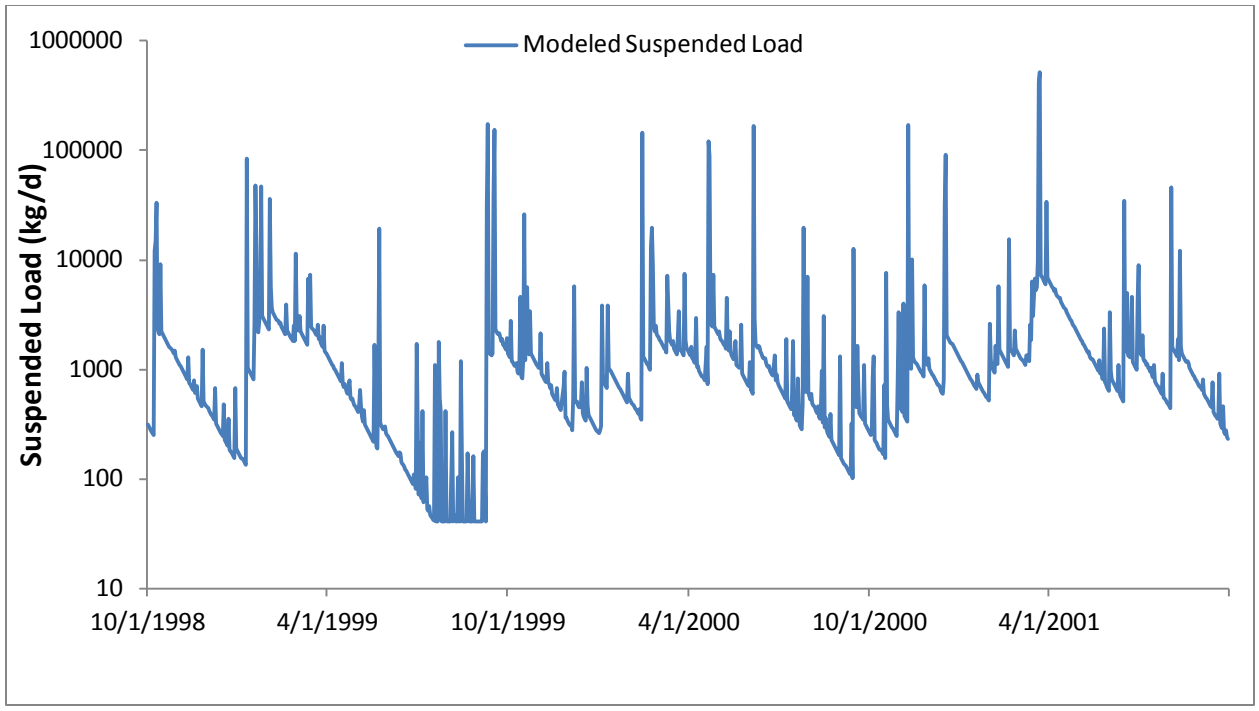

Figure 4.6 GWLF/WASP modeled daily suspended sediment load 1998-2001.

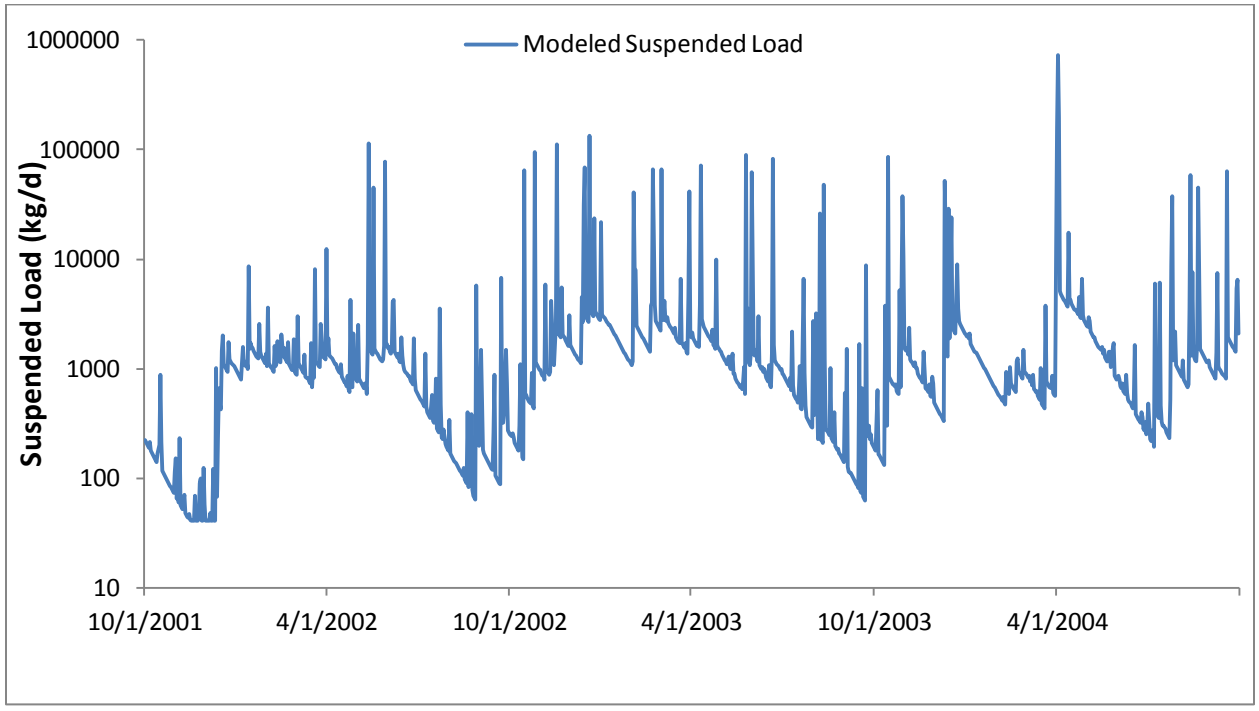

Figure 4.7 GWLF/WASP modeled daily suspended sediment load 2001-2004.

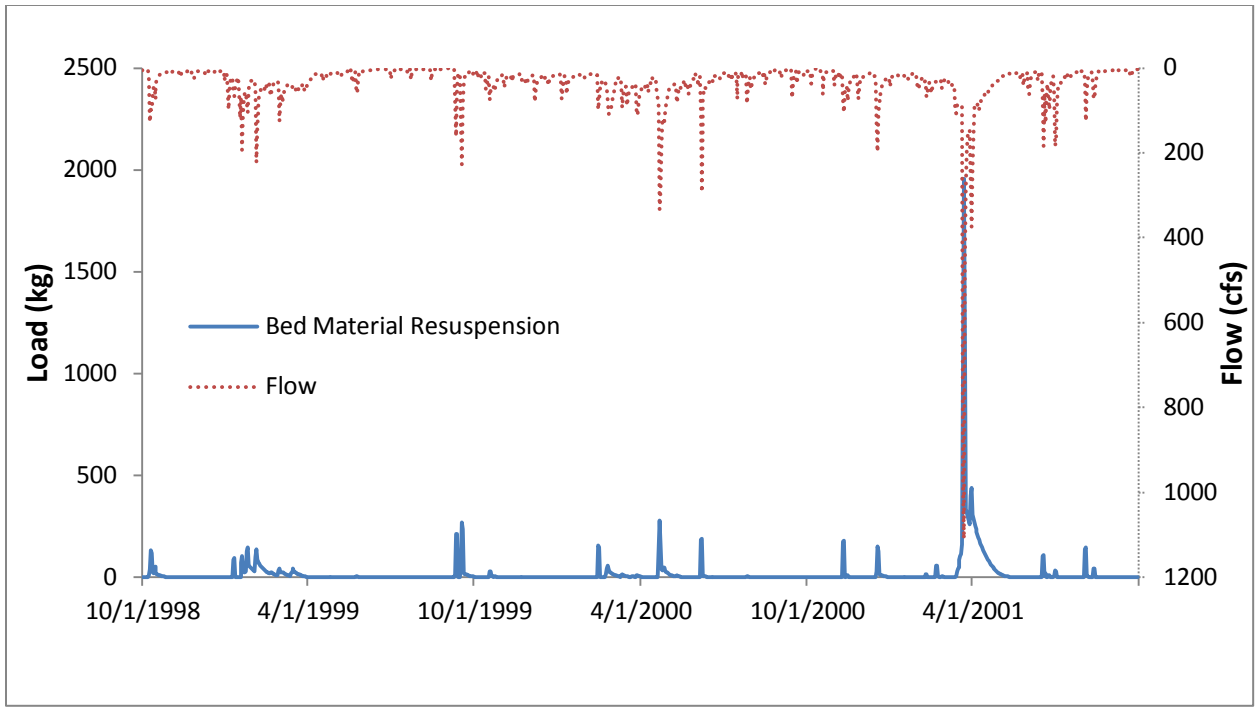

Figure 4.8 GWLF/WASP modeled daily bed material resuspension 1998-2001.

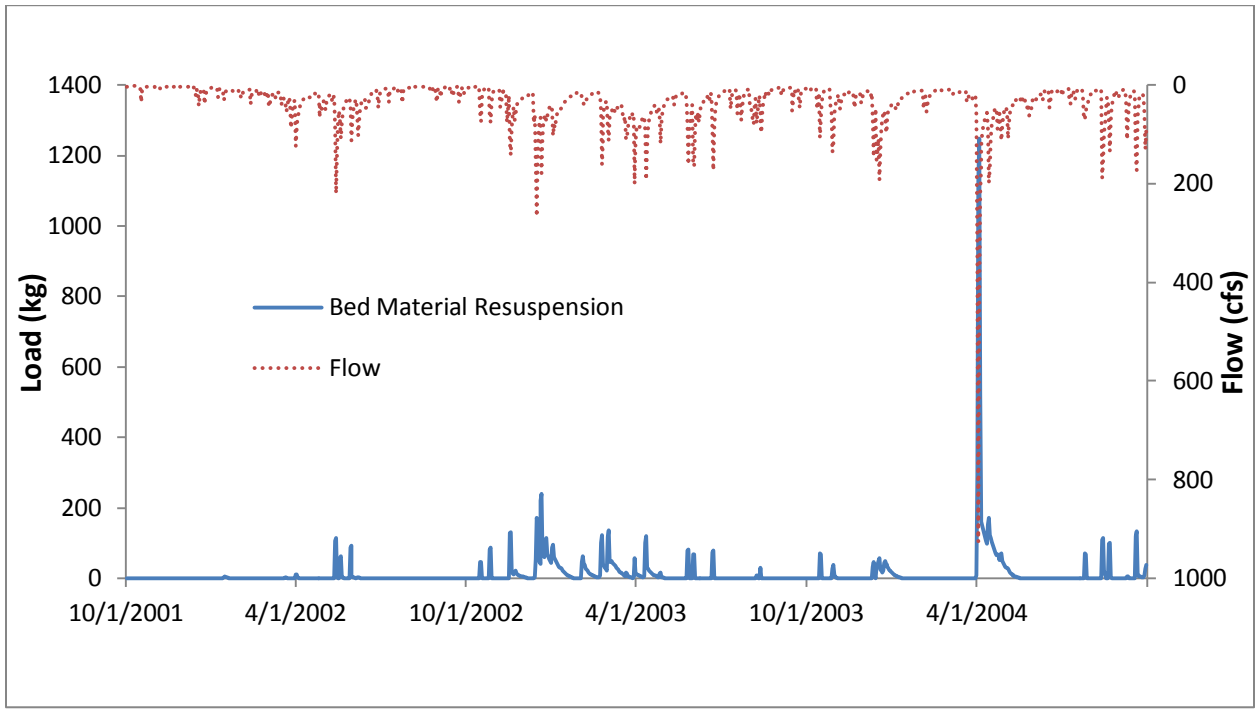

Figure 4.9 GWLF/WASP modeled daily bed material resuspension 2001-2004.

4.4 Sensitivity Analysis

As described in Chapter 4.2, bed shear stress is the critical factor determining how much bed sediment can be resuspended. Assuming that the channel geometry and bed material composition of the river remains relatively constant, the bed shear stress will then be controlled by the flow condition. Therefore, a sensitivity analysis was conducted to decide the modeled resuspension response to the changes of flow condition. The Aberjona River's flow condition from October, 1998 to September 2004 was set as the original condition. Table 4.4 listed the percentage of increase of resuspension compared to the original condition response to the increase of flow.

Table 4.4 Modeled increase of load from resuspension respond to flow increase.

Month	Flow +10%	Flow +20%	Flow +30%	Flow +40%
Jan	32.2%	67.4%	106.4%	149.3%
Feb	31.4%	65.7%	103.4%	144.3%
Mar	18.3%	37.6%	57.9%	79.2%
Apr	19.2%	38.2%	57.7%	78.0%
May	35.8%	76.8%	123.8%	176.7%
Jun	25.0%	53.0%	84.9%	121.0%
Jul	32.9%	69.9%	112.3%	162.3%
Aug	23.4%	48.5%	75.7%	105.5%
Sep	23.3%	48.1%	74.4%	102.6%
Oct	31.0%	65.5%	103.5%	145.3%
Nov	25.7%	54.3%	87.2%	124.8%
Dec	26.5%	54.1%	83.4%	114.6%
Annual	22.9%	46.9%	72.7%	100.4%

Annual load from bed material resuspension increased about 23-25% when flow was increased 10% (Figure 4.10). However, monthly results showed high variability and nonlinearity. As depicted by Figure 4.11, 10% increase of flow can lead to 18-33% increase of resuspended sediment while 40% increase of flow can result in 78-177% increase of resuspended sediment.

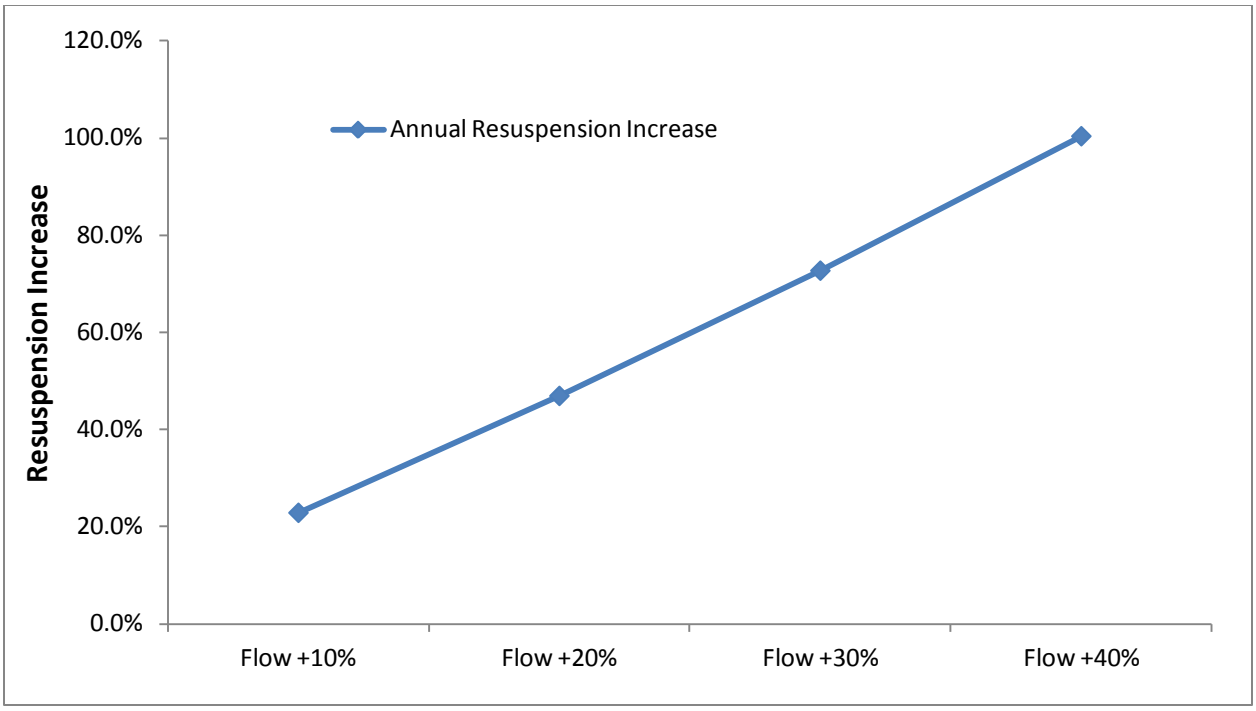

Figure 4.10 Sensitivity analysis (annual resuspension respond to flow condition).

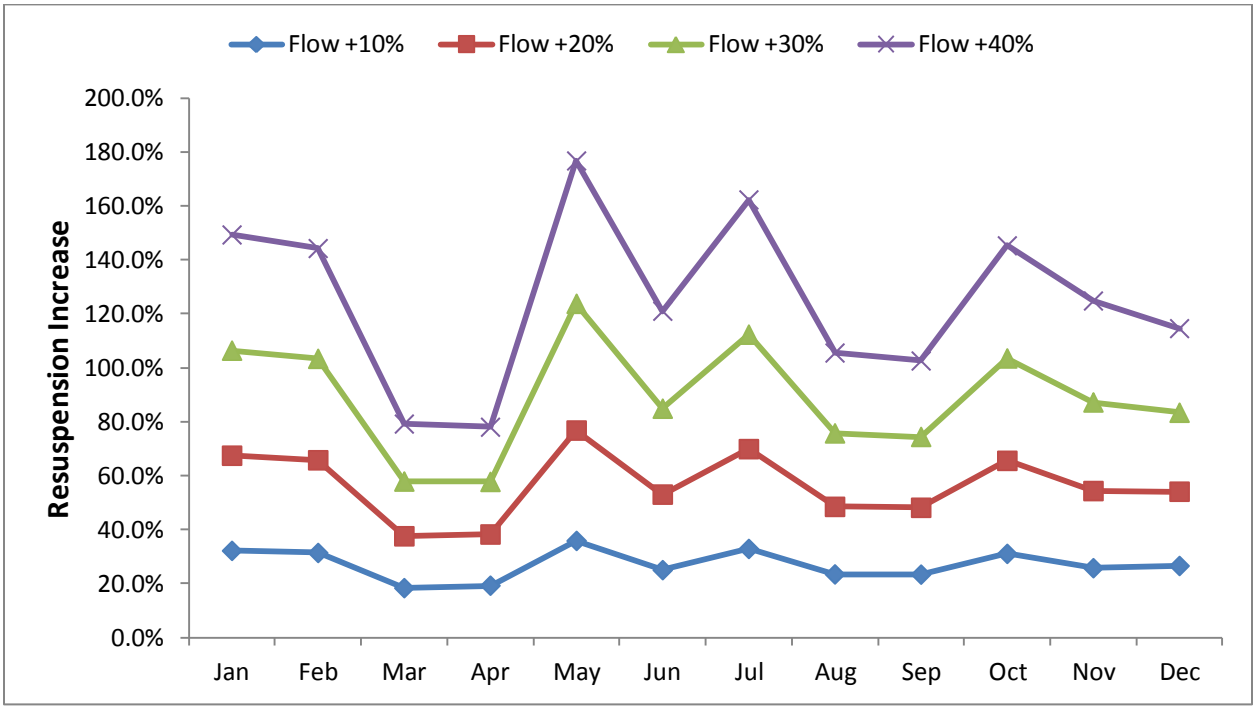

Figure 4.11 Sensitivity analysis (monthly resuspension respond to flow condition).

5 Model Application to Climate Change Scenario

5.1 Climate Change Scenario

Socio-economic and emission scenarios are alternative images of how the future might unfold and an appropriate tool to analyze how driving forces including: demographic development, socio-economic development, energy and land use, technological change, and air pollutants, may influence future greenhouse gas (GHG) emission outcomes and to assess the associated uncertainties (Nakicenovic et al., 2000). For better comparisons between various studies as well as easier communication of model results, climate research community prefers to use common sets of scenarios. These widely used sets of scenarios include the IS92 scenarios(Leggett et al., 1992), SRES scenarios (Nakicenovic et al., 2000) and most recently, Representative Concentration Pathways (RCPs) scenarios (Vuuren et al., 2011).

This study employed RCPs scenarios for its climate change analysis. The four RCPs (Table 5.1) cover a wide range of the existing literature for radiative forcing values and most other variables. The resulting product forms a comprehensive data set with high spatial and sectoral resolutions for the period extending to 2100 (Vuuren et al., 2011).

Table 5.1 Main characteristics of each RCP (Vuuren et al., 2011).

Scenario Component	RCP2.6	RCP4.5	RCP6	RCP8.5
Greenhouse gas emissions	Very low	Medium-low mitigation; Very low baseline	Medium baseline; High mitigation	High baseline
Agricultural area	Medium for cropland and pasture	Very low for both cropland and pasture	Medium for cropland but very low for pasture	Medium for both cropland and pasture
Air Pollution	Medium-low	Medium	Medium	Medium-high

5.2 Climate Projections Selection

The World Climate Research Program (WCRP) develops global climate projections through its Coupled Model Intercomparison Project (CMIP). During 2012-2013, WCRP released its latest global climate projections from CMIP phase 5 (CMIP5) (Brekke et al., 2013). Since global climate projections generally have a horizontal resolution of 100 kilometers or greater, for local impacts assessment such as in this study, downscaled CMIP5 climate projections were chosen. WCRP have applied two statistical downscaling techniques – monthly bias-correction and spatial disaggregation (BCSD) and daily bias-correction and constructed analogs (BCCA) to a large ensemble of new climate projections released through the CMIP5 (Brekke et al., 2013). Table 5.2 listed all sets of downscaled projections currently available on CMIP5 website for the study area (Grid boundary latitude: 42.375°, 42.5°; longitude: -71.25°, -71.125°).

Table 5.2 Available downscaled CMIP5 projections.

Climate Models	RCP2.6	RCP4.5	RCP6.0	RCP8.5	Total
access1-0		1		1	2
bcc-csm1-1	1	1	1	1	4
bnu-esm		1		1	2
canesm2	5	5		5	15
ccsm4	2	2	2	2	8
cesm1-bgc		1		1	2
cnrm-cm5		1		1	2
csiro-mk3-6-0	10	10		10	30
gfdl-cm3	1		1	1	3
gfdl-esm2g	1	1	1	1	4
gfdl-esm2m	1	1	1	1	4
inmcm4		1		1	2
ipsl-cm5a-lr	3	4	1	4	12
ipsl-cm5a-mr	1	1	1	1	4
miroc5	3	3	1	3	10
miroc-esm	1	1	1	1	4
miroc-esm-chem	1	1	1	1	4
mpi-esm-lr	3	3		3	9
mpi-esm-mr	1	3		1	5
mri-cgcm3	1	1	1	1	4

noresm1-m	1	1	1	1	4
Grand Total	**36**	**43**	**13**	**42**	**134**

Each CMIP5 BCCA projection has three sets of daily variables (precipitation, minimum and maximum surface air temperature). To simplify subsequent model simulation, three representative projections were selected from 134 projections based on their maximum 2-day precipitation and mean annual temperature for the period of 2030-2059 (middle of century) and 2070-2099 (end of century) to cover the range of variability in precipitation and temperature among all projections.

Table 5.3 Climate projection feature.

Name	GCM	RCP
Low	IPSL-CM5A-LR	RCP4.5
Mid	CSIRO-Mk3.6.0	RCP8.5
High	MIROC-ESM-CHEM	RCP8.5

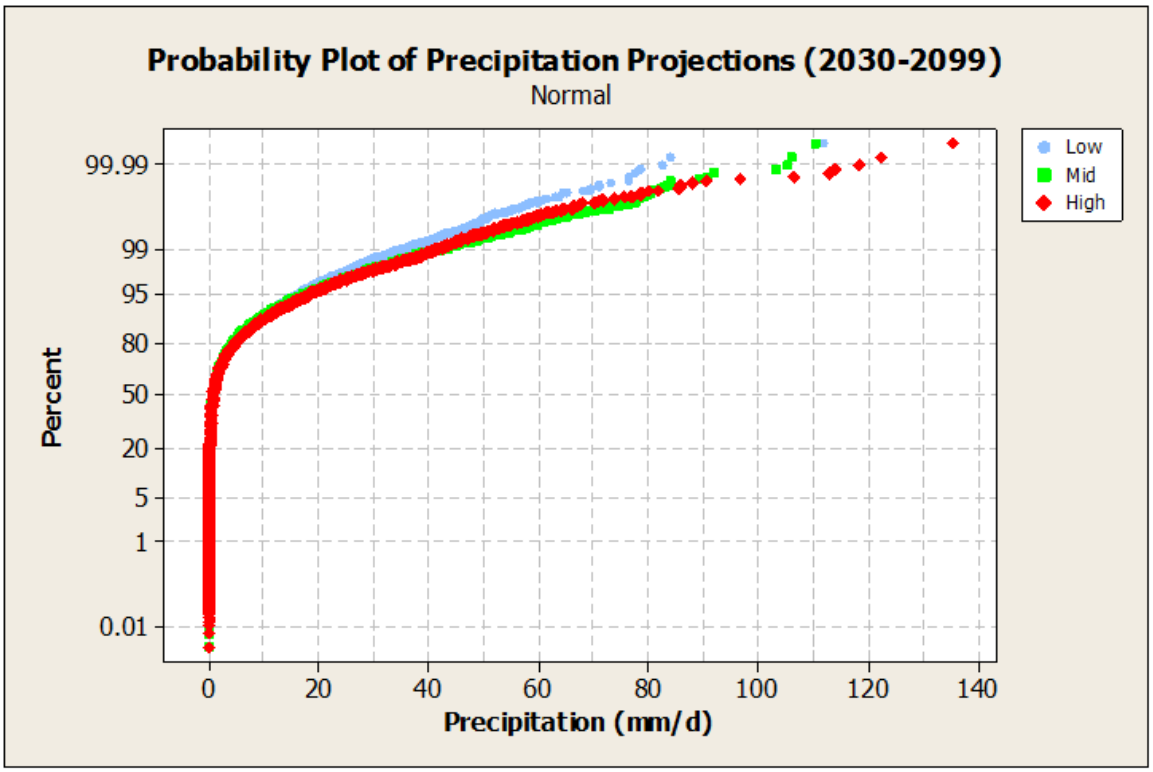

Figure 5.1 Cumulative distribution of precipitation projections (2030-2099).

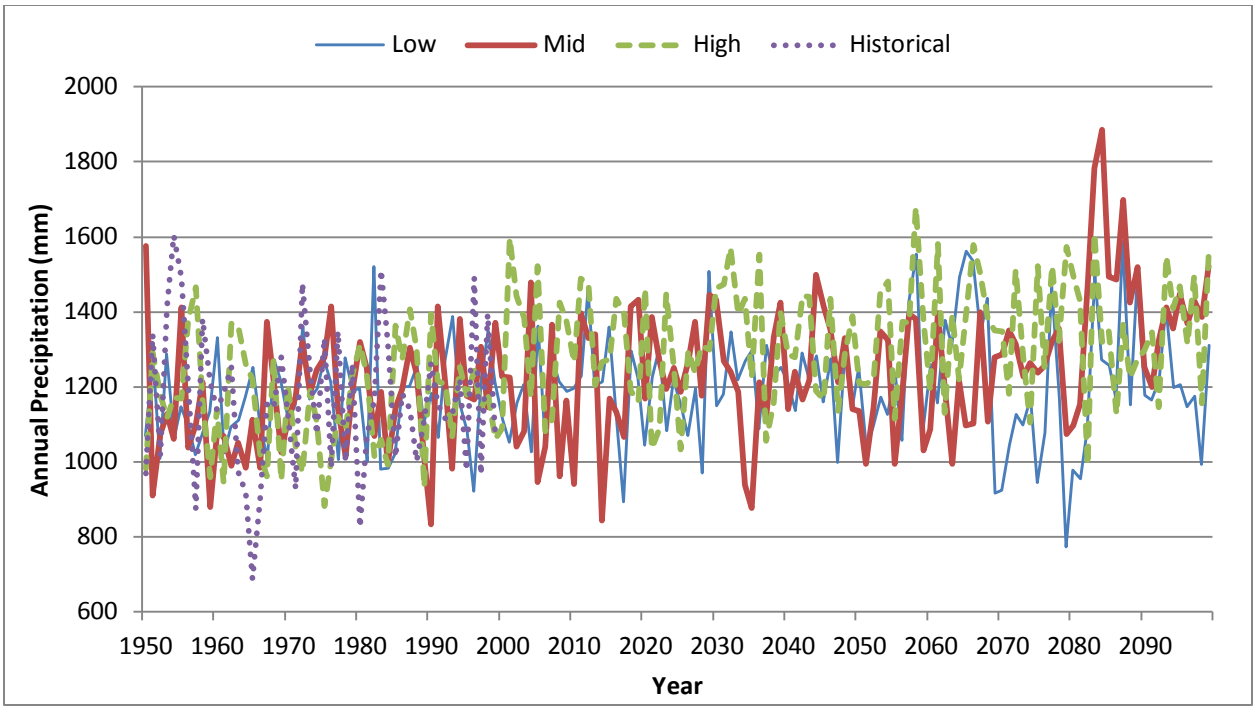

Figure 5.2 Annual precipitation. Historical: data from NCDC station at Reading, MA; Low, Mid and High: GCM projections downloaded from CMIP5 website.

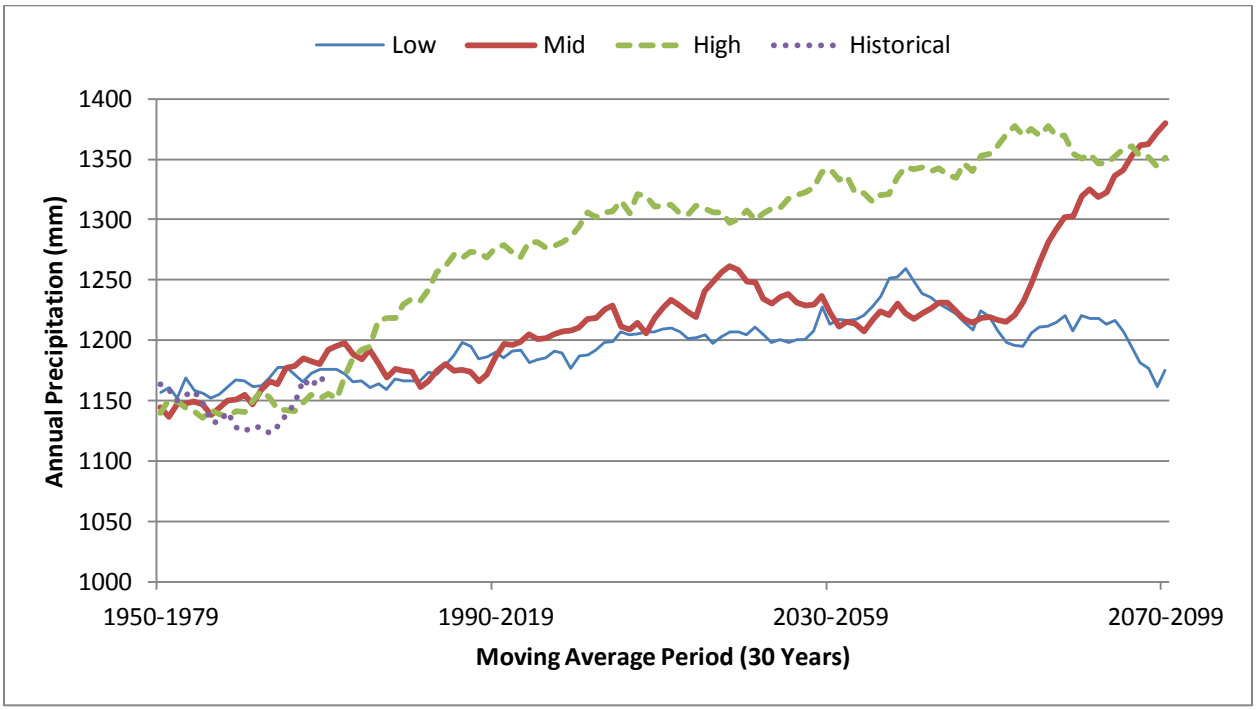

Figure 5.3 Annual precipitation moving average.

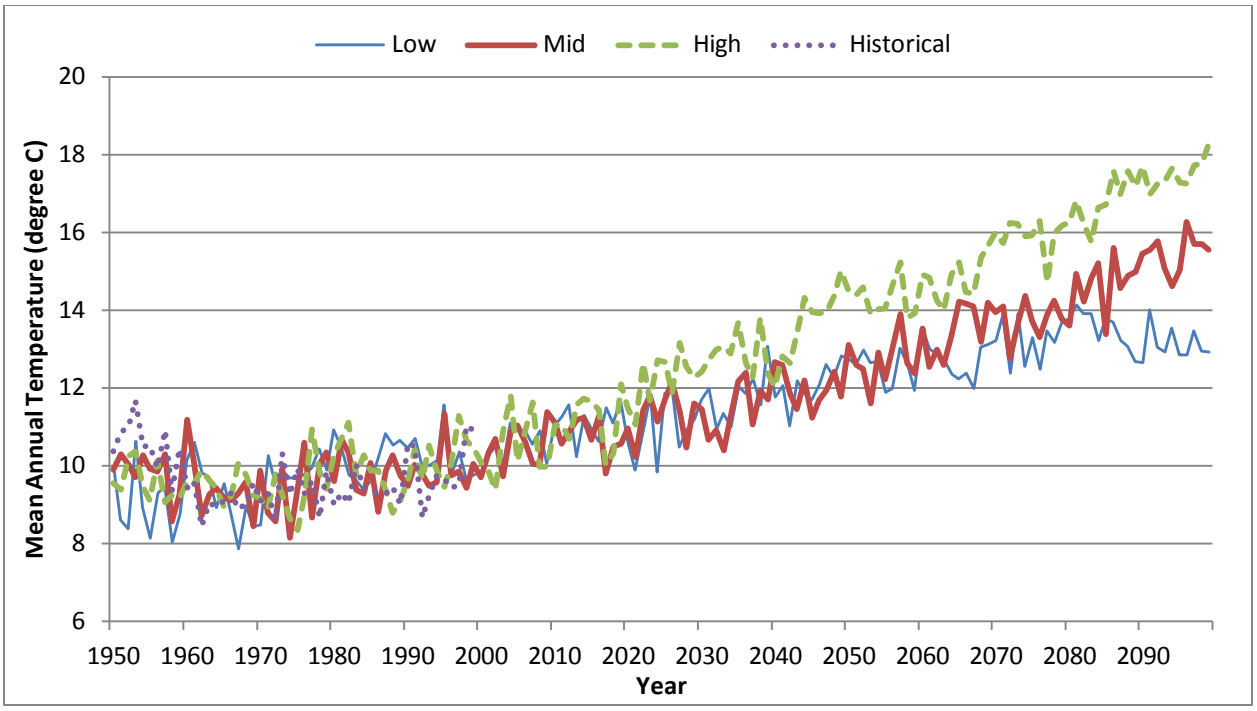

Figure 5.4 Mean annual temperature. Historical: data from NCDC station at Reading, MA; Low, Mid and High: GCM projections downloaded from CMIP5 website.

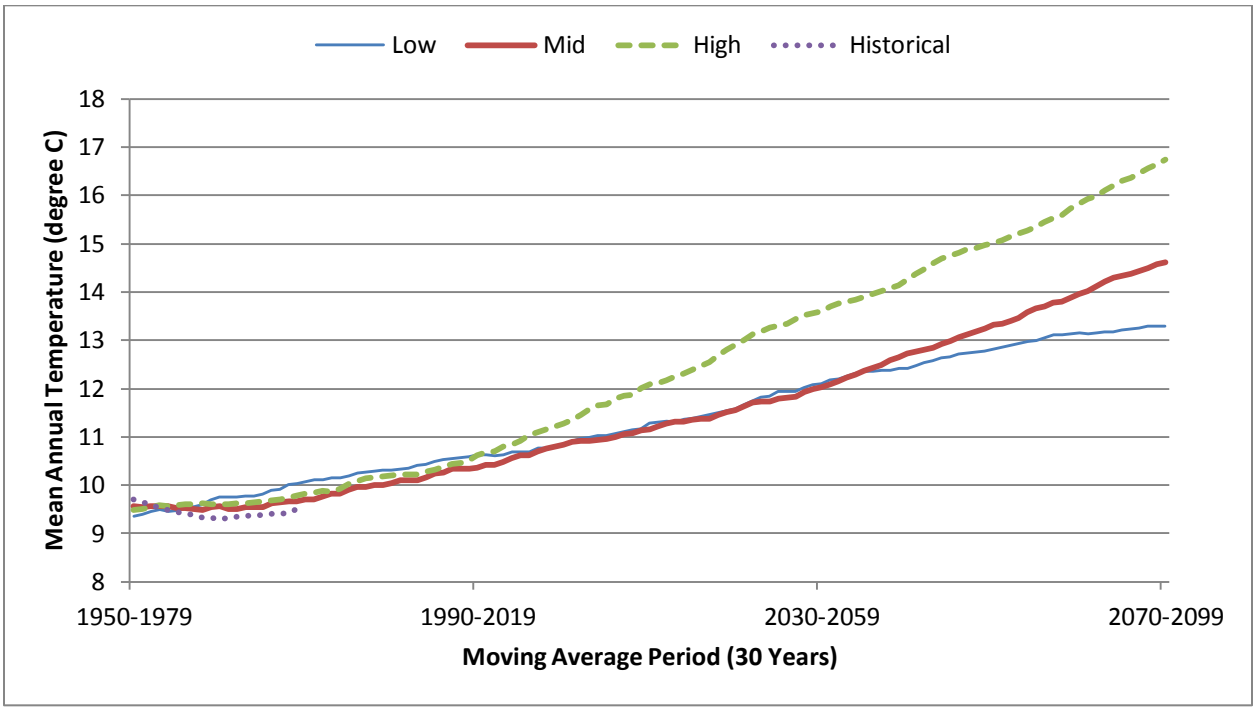

Figure 5.5 Mean annual temperature moving average.

Figure 5.1 showed that the daily maximum precipitation projection for future period 2030-2099 ranges from 80-135 mm/d and the High scenario have largest storm event among three in terms of both magnitude and frequency. Figure 5.3 indicated that in the middle of the century, annual rainfall is projected to increase about 50-170 mm/year compared to historical observation (1950-1999), while by the end of the century, 10-220 mm/year. (All plotted BCCA daily precipitation projections were bias corrected following the suggestion by Downscaled CMIP5 Errata (Brekke, 2013)). As depicted by Figure 5.5, mean annual temperature is predicted to increase 2.3-3.9 ℃ by the mid century while 3.6-7.0 ℃ by the end of the century.

5.3 Model Application and results comparison

The integrated model was run for historical climate data (1950-1999) and three GCM climate projections (1950-2099). The results and the moving averages were displayed by Figure 5.6 through Figure 5.15 ("Historical" case in these figures (dotted line) represented the modeled results with observed climate data as input). Annual results comparison was shown in Table 5.4.

Table 5.4 Annual results (moving average) comparison.

Variable	*Period*	*Low*	*Change*[3]	*Mid*	*Change*[3]	*High*	*Change*[3]
Annual Precipitation	2030-2059	12.1	4.53%	12.2	5.33%	13.4	15.62%
(11.6×10^2 mm)[1]	2070-2099	11.7	1.22%	13.8	18.91%	13.5	16.41%
Mean Annual Temperature	2030-2059	12.1	25.26%	12.0	24.37%	13.6	40.79%
(9.7 ℃)[1]	2070-2099	13.3	37.47%	14.6	51.28%	16.7	73.14%
Mean Annual Flow	2030-2059	32.0	-15.04%	34.2	-9.17%	35.5	-5.67%
(37.7 cfs)[2]	2070-2099	28.8	-23.58%	37.7	0.00%	31.7	-15.83%
Annual Suspended Load	2030-2059	1.10	-2.44%	1.24	9.64%	1.35	19.05%
(1.13 Gg)[2]	2070-2099	1.04	-8.22%	1.49	32.15%	1.34	18.15%
Annual Resuspension	2030-2059	4.29	8.29%	5.54	40.01%	6.00	51.59%
(3.96 Mg)[2]	2070-2099	4.06	2.45%	7.46	88.59%	4.68	18.14%

[1]Number in parenthesis is the mean of historical observation from 1950-1999; [2]Number in parenthesis is the mean of modeled results with historical P and T from 1950-1999 as input; [3]Changes are based on the number in parenthesis in the first column.

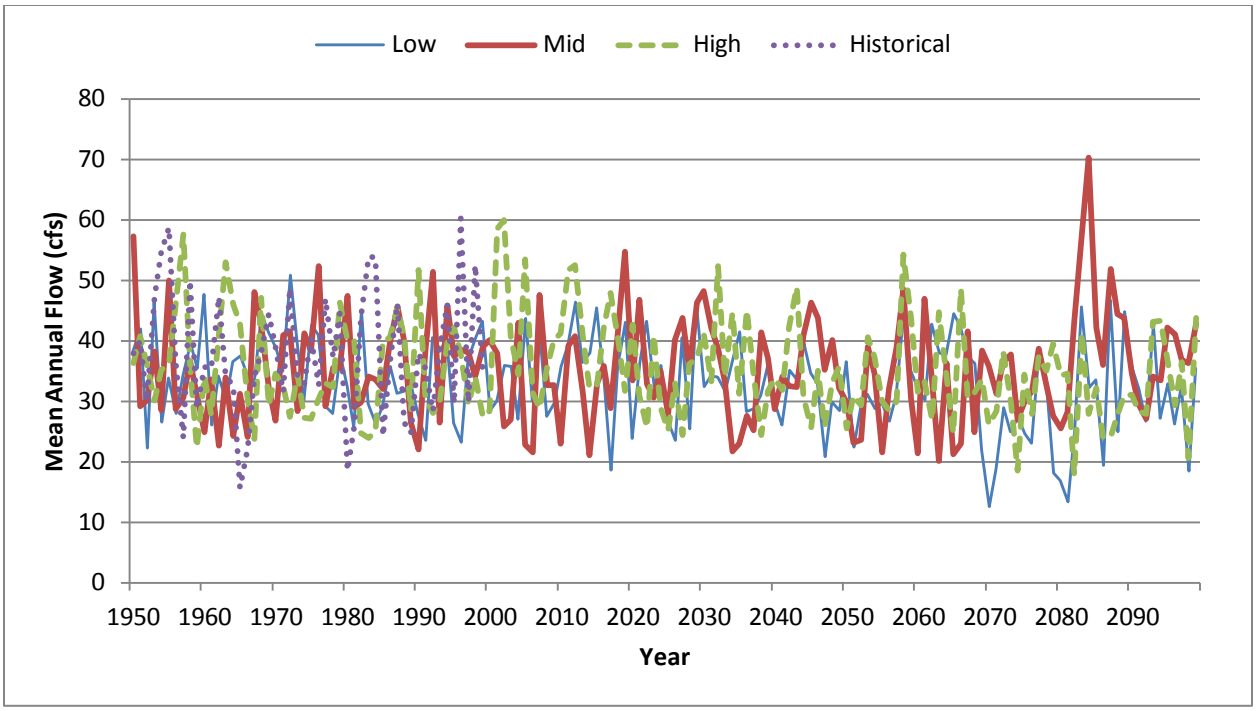

Figure 5.6 Mean annual flow. Historical: displayed the GWLF/WASP simulated result with historical NCDC climate data as input. Low, Mid and High: showed the GWLF/WASP simulated results under three representative climate scenarios.

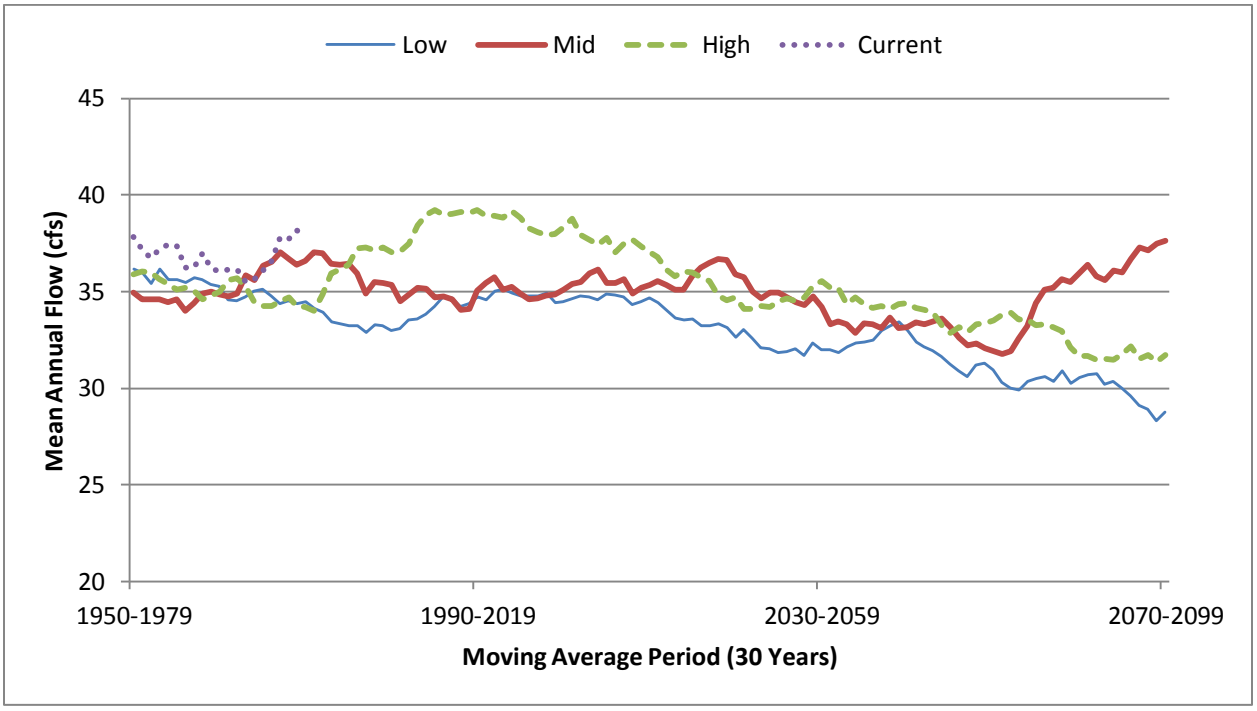

Figure 5.7 Mean annual flow moving average.

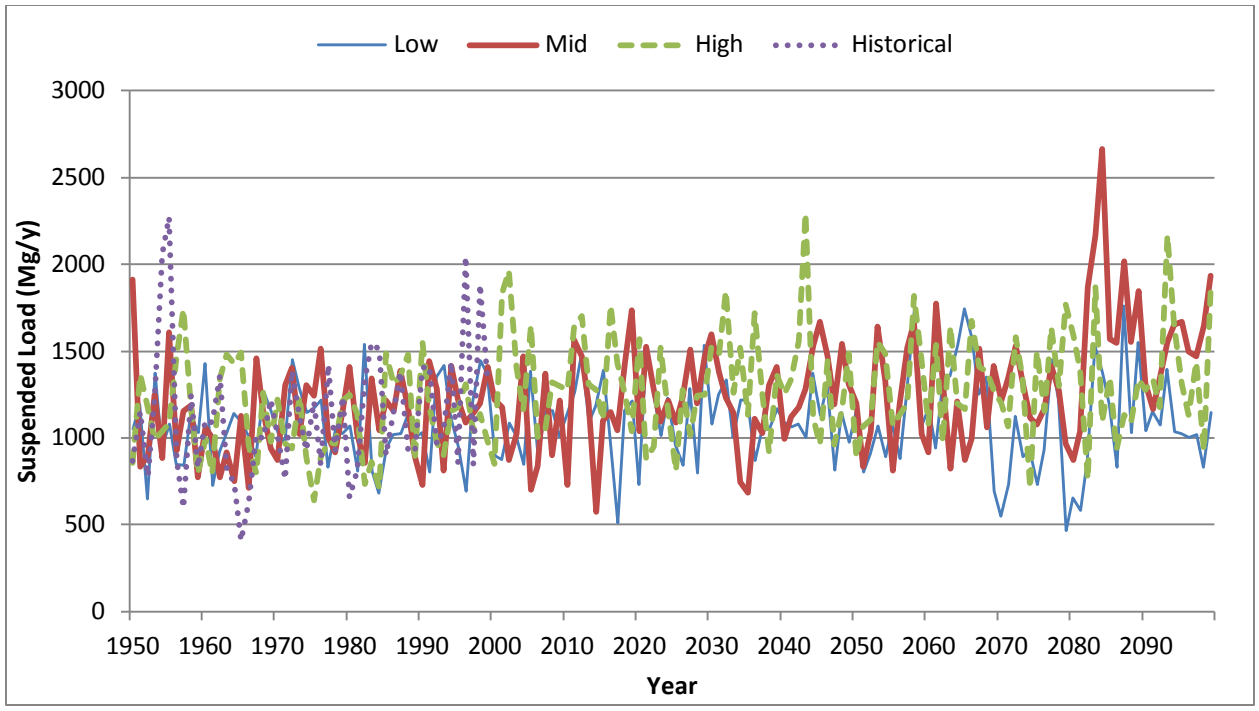

Figure 5.8 Annual suspended load. Historical: displayed the GWLF/WASP simulated result with historical NCDC climate data as input. Low, Mid and High: showed the GWLF/WASP simulated results under three representative climate scenarios.

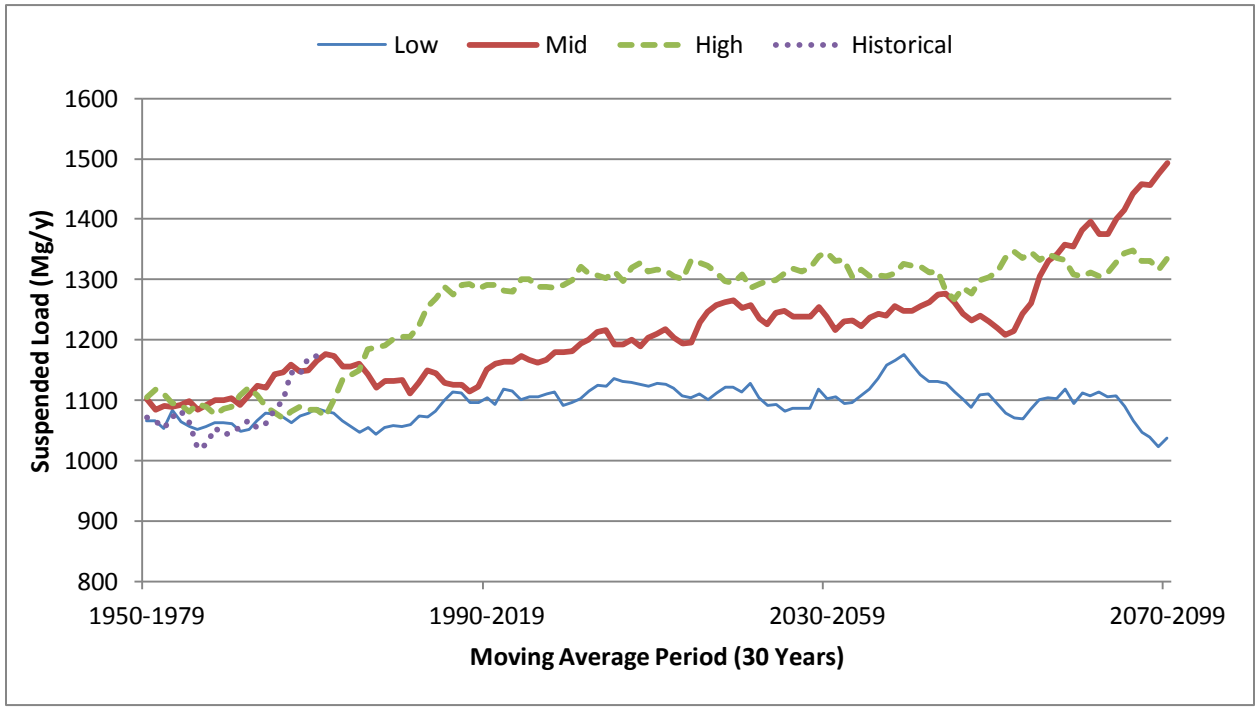

Figure 5.9 Annual suspended load moving average.

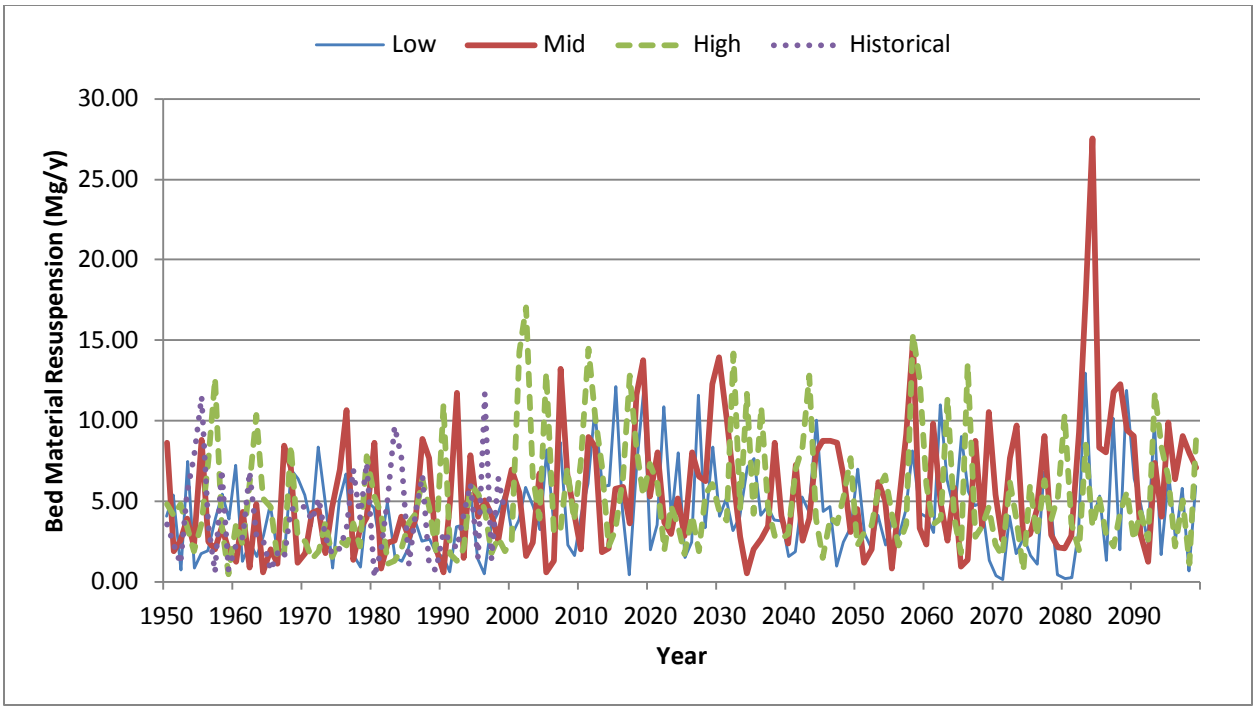

Figure 5.10 Annual bed material resuspension. Historical: displayed the GWLF/WASP simulated result with historical NCDC climate data as input. Low, Mid and High: showed the GWLF/WASP simulated results under three representative climate scenarios.

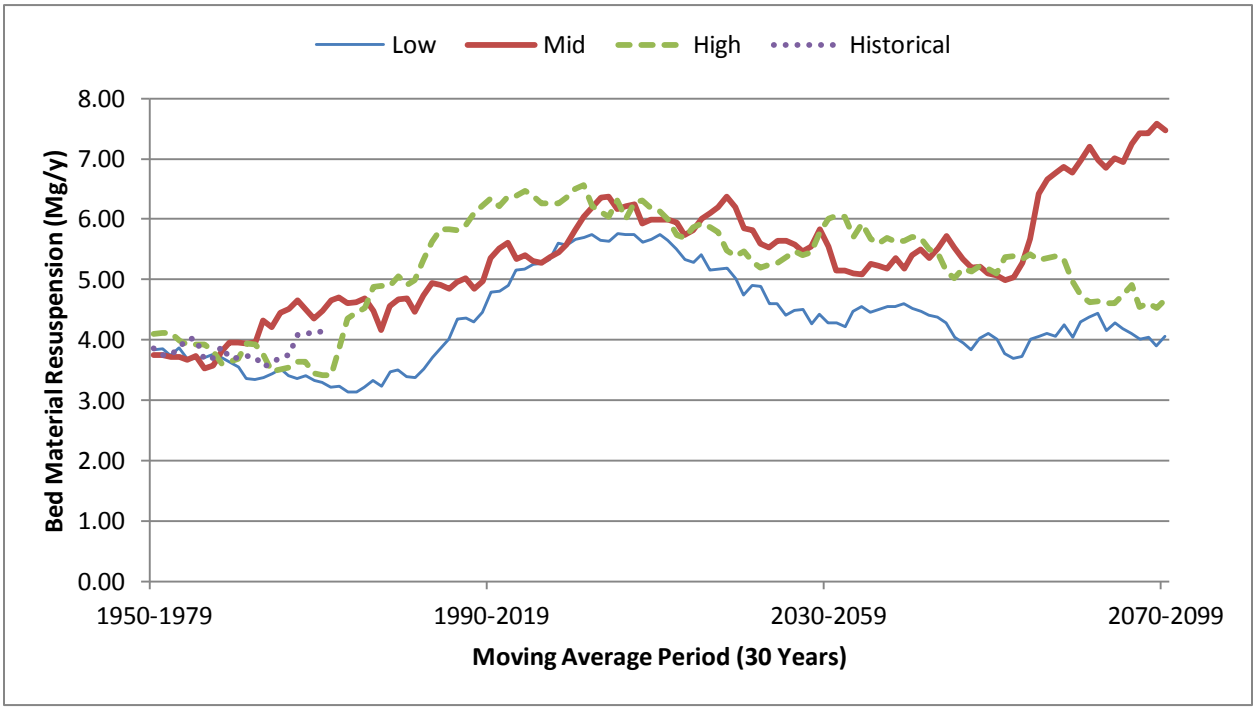

Figure 5.11 Annual bed material resuspension moving average.

For the Low scenario, annual rainfall remained at the historical level while a mild warming trend is expected by the end of the century. Meanwhile, the mean flow and suspended load decreased 24% and 8% respectively and total bed material resuspension remained at the historical level. This suggested that resuspension was limited primarily by the high flow condition or transport capacity.

With respect to the High scenario, annual precipitation increased about 16.4% though, mean annual flow lowered 16% by the century end. This can mainly be attributed to the scenario's drastic warming trend which intensified evapotranspiration significantly that counteracted the increase of rainfall. Even so, suspended load and resuspension still went up both about 18%. For the Mid scenario, annual rainfall went up 19% while flow remained at the historical level due to the mediate-high temperature rise by the end of the century. However, the suspended load and resuspension increased dramatically by 32% and 89%.

Comparing the results of the Mid and High scenarios, increase of resuspension clearly indicated that extreme storm events appeared with higher intensity and frequency in both cases. Meanwhile, increase of suspended load in both cases can mainly be addressed to the increase of wash load resulted from more rainfall. But the extent of increase was different since the change of evapotranspiration caused by the temperature rise varied between the two scenarios. Further explanation of the processes may come from analyzing the monthly behavior of the system.

In terms of TSS concentration, more damage to water quality was indicated by the modeled results (Figure 5.12 through Figure 5.15). According to EPA, most States only have narrative water quality criteria (WQC) for sediments of the form: "Surface waters shall be free from pollutants in amounts that cause objectionable conditions or impairment of designated uses". Only a few States use numeric TSS criteria which vary from 30 mg/L up to 158 mg/L

(USEPA, 2006). Therefore, the numbers of days which mean daily TSS exceeded 30 mg/L and 100 mg/L (named by N_{30} and N_{100}) were counted respectively to reflect sediment level trend. As displayed by Table 5.5, high transient TSS concentrations did occur more frequently under future climate scenario with high temporal variability. Under the High scenario, a typical wet year had N_{30} = 30 days and N_{100} = 10 days while historically N_{30} = 25 days and N_{100} = 8 days.

Table 5.5 Results of TSS.

Scenario	Moving Average Period	No. of days TSS>30mg/L	No. of days TSS>100mg/L
Historical	1950-1990	17	5
Low	2030-2059	18	5
	2070-2099	19	5
Mid	2030-2059	17.5	5.5
	2070-2099	19	6.5
High	2030-2059	19	6.5
	2070-2099	22	7

Comparing Figure 5.8 to Figure 5.10, in terms of total amount, wash load remained to be the main source of suspended sediment load for most of the time since it was several magnitudes larger than bed material resuspension and resuspension was rarely discernible for most small and moderate rainfall events. However, it is still necessary to consider resuspension during extreme rainfall event because wash load is limited by the availability of eroded soil on the watershed land surface while resuspension is controlled by the flow condition. So for a large rainfall event with a relatively longer duration, surface runoff occurring after the "first flush" process will not bring that much wash load as the beginning of the storm because there is no eroded soil available. But they may still generate large flow later which exerts higher shear stress on the river bed and resuspension may become the major source of suspended sediment then. As mentioned in Chapter 4.2.1, since only daily precipitation projection is available, the integrated model does not have the capacity to predict what time in one certain day did the wash-off

process begin and its duration. So it is misleading to attribute any specific day's abnormal TSS concentration only to wash load or bed material resuspension. But the model can still project the general trend of both wash load and resuspension under future climate scenario with adequate accuracy.

It should be noted that the results showed in Figure 5.10 and 5.11 only reflected the resuspension from Aberjona mainstream. The model cannot determine the bed material resuspension from the river's tributaries mechanistically since the model only simulate hydrodynamic in the mainstream. Moreover, this GWLF/WASP model calculated resuspension velocity using a conservative equation (Chapter 4.2) which may lead to an underestimation. To better understand the relationship between resuspension and flow condition, field measurement of resuspension needs to be conducted to choose the best suitable empirical equation or create a new one for the Aberjona River specifically. And stormwater sampling must be done to validate the model's prediction of wash load and resuspension.

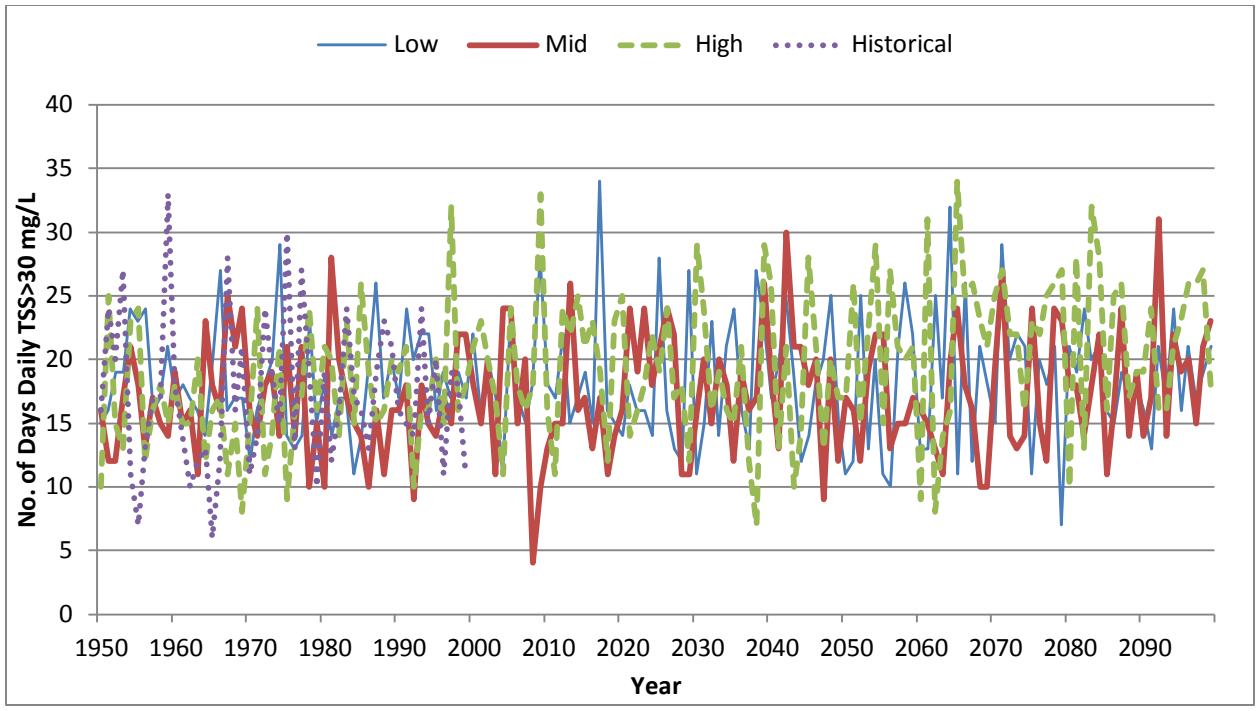

Figure 5.12 Number of days per year when daily TSS>30 mg/L (N_{30}). Historical: displayed the GWLF/WASP simulated result with historical NCDC climate data as input. Low, Mid and High: showed the GWLF/WASP simulated results under three representative climate scenarios.

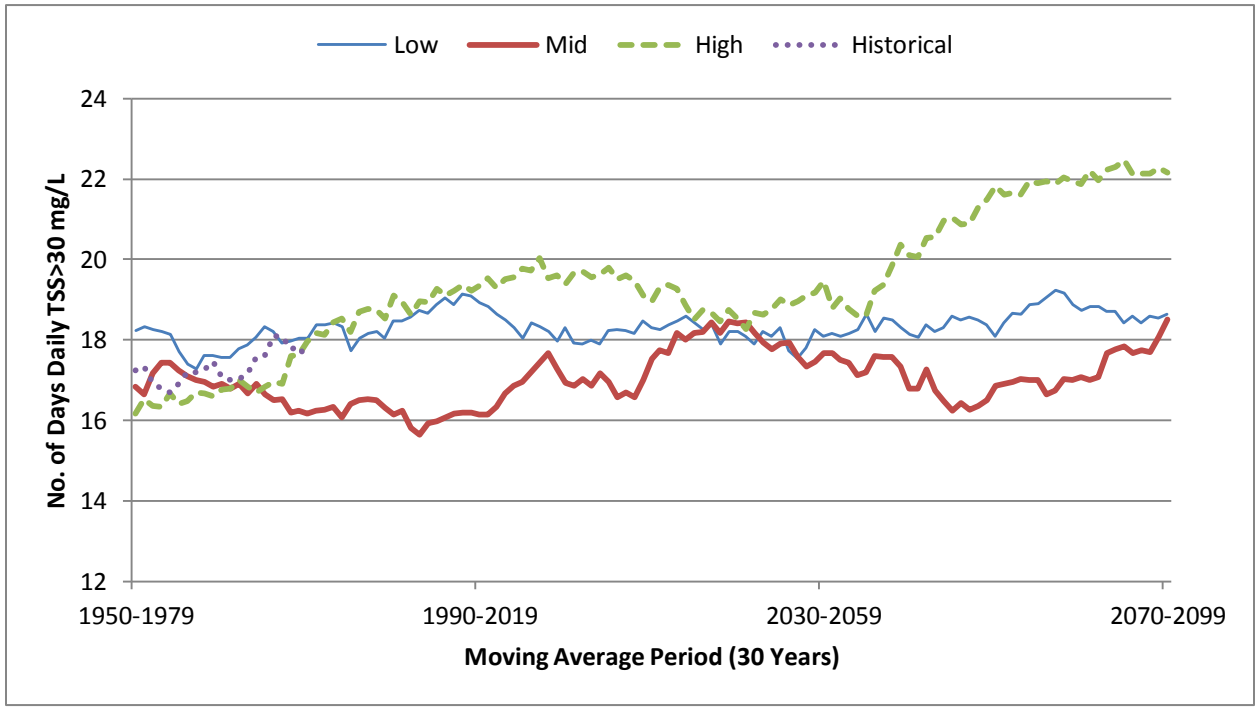

Figure 5.13 Number of days per year when daily TSS>30 mg/L (N_{30}) moving average.

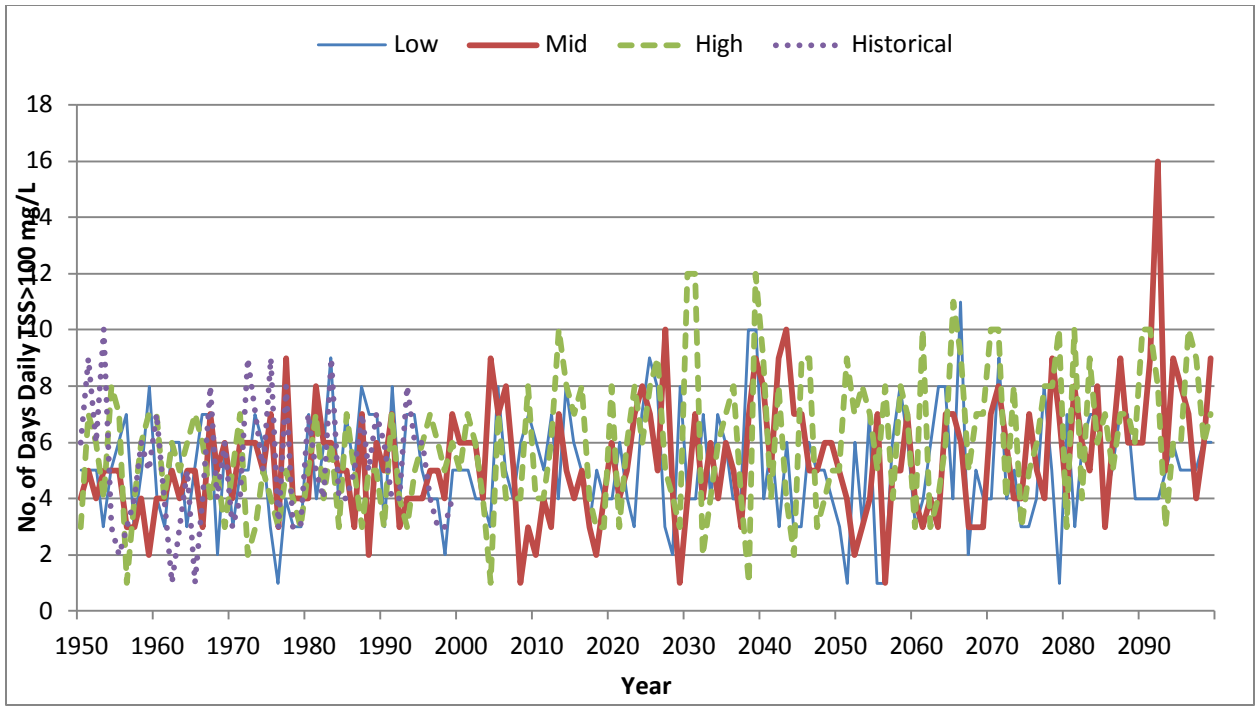

Figure 5.14 Number of days per year when daily TSS>100 mg/L (N_{100}). Historical: displayed the GWLF/WASP simulated result with historical NCDC climate data as input. Low, Mid and High: showed the GWLF/WASP simulated results under three representative climate scenarios.

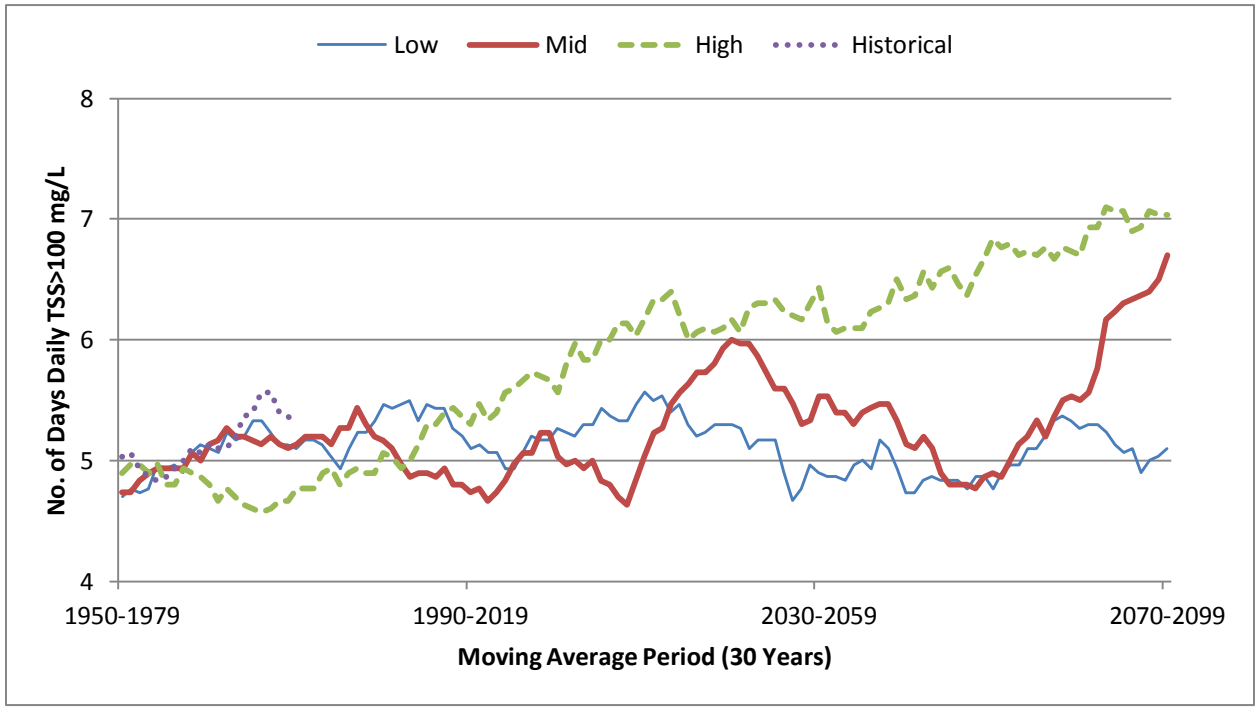

Figure 5.15 Number of days per year when daily TSS>100 mg/L (N_{100}) moving average.

5.4 Monthly Change Analysis

As displayed by Figure 5.16 (For Figure 5.16 through Figure 5.20, MC stands for Mid-century and EC stands for end of century), mean monthly temperature increased by 1.5 to 5 °C by the Mid-century while 2.9 to 8.2 °C by the end of the century depending on climate scenario.

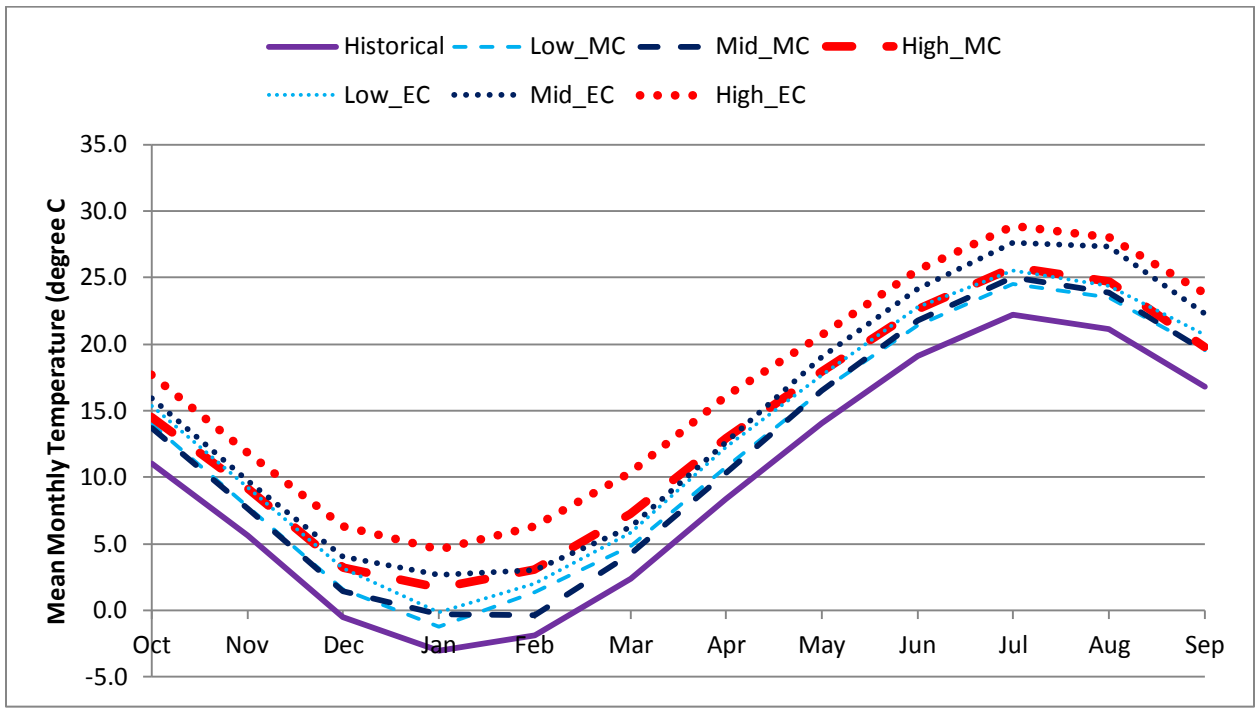

Figure 5.16 Monthly temperature. EC: end of century; MC: mid-century; Historical: displayed the GWLF/WASP simulated result with historical NCDC climate data as input; Low, Mid and High: showed the GWLF/WASP simulated results under three representative climate scenarios.

Monthly precipitation increased significantly in winter (Dec. & Jan.) while decreased in summer (Jul. & Aug.) for all scenarios. Other months showed high variability depending on the scenarios and their time periods (Figure 5.17). Mean monthly suspended load is modeled to change by -87% to 140% for the Mid-century and by -87% to 164% for the end of the century (Figure 5.18). The change in monthly suspended load generally corresponded to the trend of precipitation which indicated a high correlation between suspended load and surface runoff volume. For the High scenario, the significant reduction of rainfall in summer resulted in less

suspended load which offset the increase of suspended load during high flow period in winter, so the annual load increased mildly. For the Mid scenario, with significant rise of rainfall in winter and slight decrease in summer, annual load increased remarkably.

According to Figure 5.19, highest mean monthly flow switched from March to February or January for most scenarios. This may due to the warming trend in winter which made the precipitation occur more in the form of rainfall rather than snow and the snowmelt process usually happen in March switched earlier. Temperature rise and precipitation decrease also leaded to the decrease of flow in summer. Change in monthly resuspension varies from -99% to 237% and -100% to 342% for the two scenario periods respectively and corresponded to the change of streamflow. Monthly resuspension increased significantly in December and January when most extreme storm event occurred while reduced in summer low flow period. For other months, resuspension varied with climate scenarios.

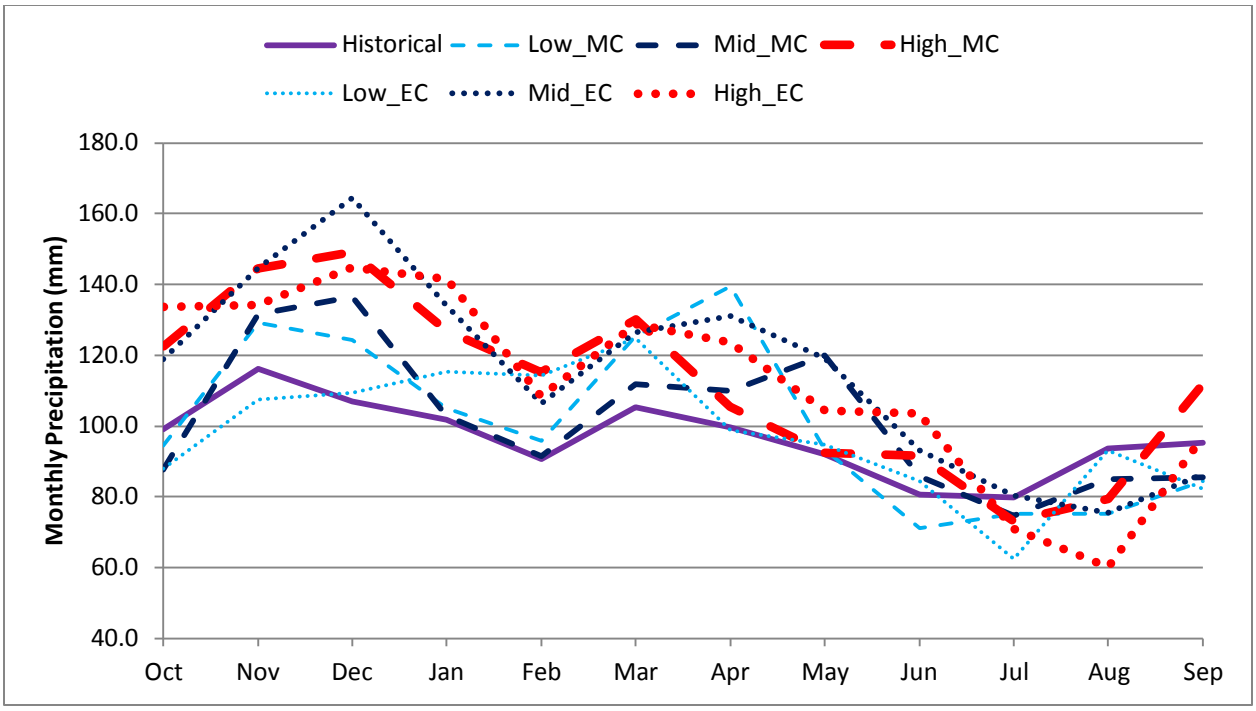

Figure 5.17 Monthly mean precipitation. EC: end of century; MC: mid-century; Historical: displayed the GWLF/WASP simulated result with historical NCDC climate data as input; Low, Mid and High: showed the GWLF/WASP simulated results under three representative climate scenarios.

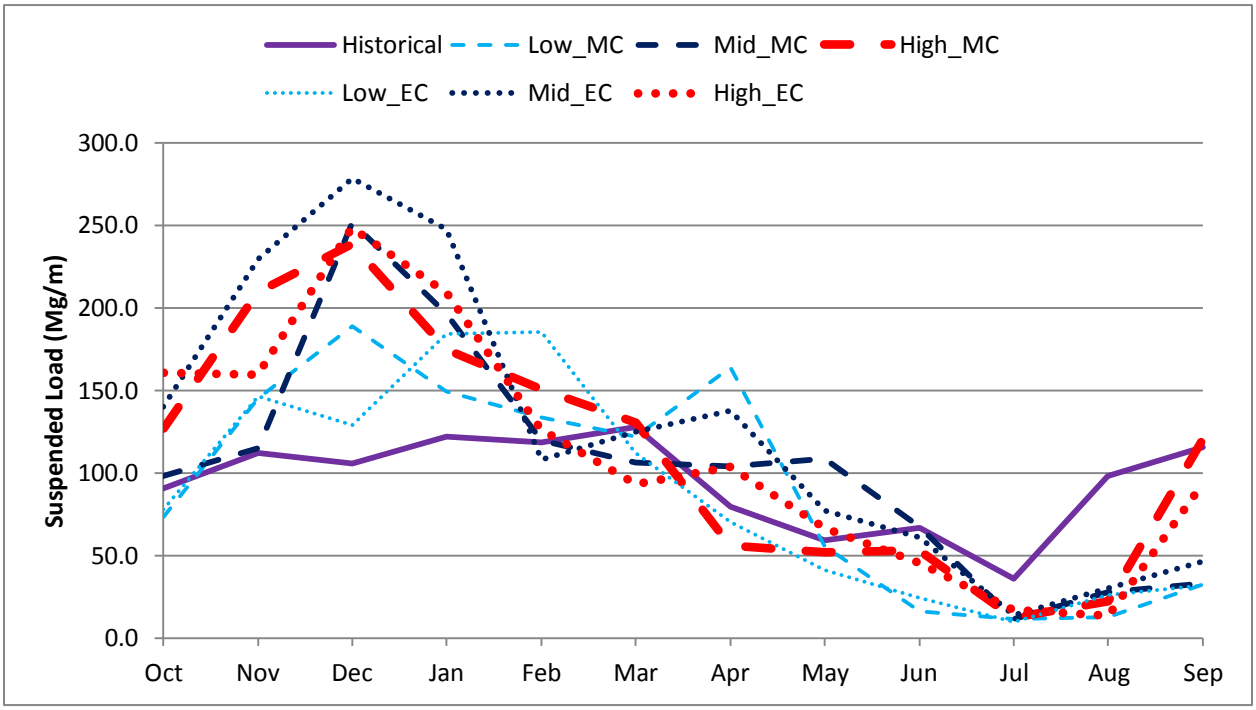

Figure 5.18 Monthly suspended load.

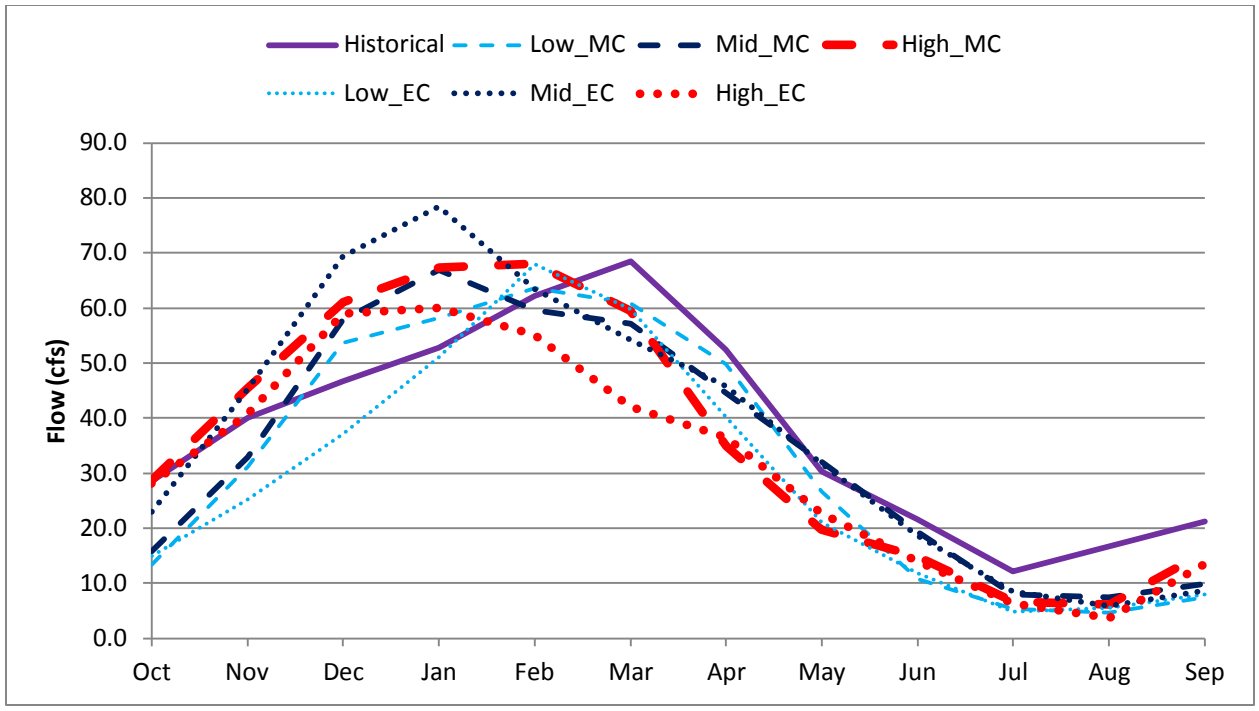

Figure 5.19 Monthly flow. EC: end of century; MC: mid-century; Historical: displayed the GWLF/WASP simulated result with historical NCDC climate data as input; Low, Mid and High: showed the GWLF/WASP simulated results under three representative climate scenarios.

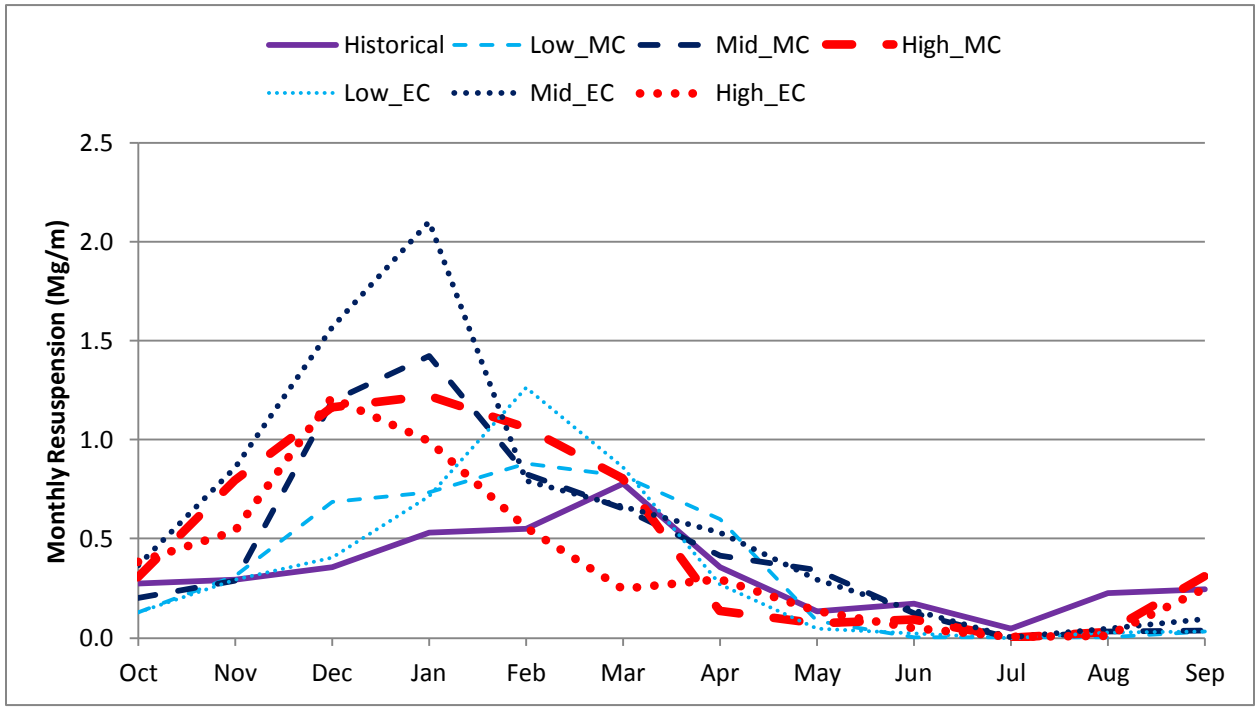

Figure 5.20 Monthly resuspension.

6 Conclusions and Recommendations

This study developed the GWLF/WASP model that simulates flow and suspended sediment load and transport reasonably well in the Aberjona River. The integrated model demonstrated adequate simulation ability with limited input data by reproducing flow condition and storm peak TSS concentration consistent with the observed data. The GWLF/WASP model also proved its prediction capacity while maintaining the model's medium complexity without addition of more parameters. Further improvements of this model should be committed to: 1) understand the occurrence and transport pattern of wash load more thoroughly by stormwater sampling; 2) direct measurement of sediment resuspension and sediment size distribution to develop site specific empirical equation for the estimation of bed material resuspension.

Climate change effect on suspended sediment load and resuspension is highly determined by the emission scenario and exhibited large variability. As shown in this research, by the middle of this century, annual suspended load in the Aberjona River changed from -2% to +19% while annual resuspension from 8% to 52% compared to the historical level. By the century end, annual resuspension varied from -8% to 32% while resuspension from 2% to 88% compared to the historical level. Monthly change showed even larger divergence and variability. Change in monthly suspended load was modeled by -87% to 140% for the Mid-century and by -87% to 164% by the end of the century. Change in monthly resuspension varies from -99% to 237% and -100% to 342% for the two scenario periods respectively. In terms of wash load, it responded more directly to the runoff volume influenced by the change of precipitation. For resuspension, extreme flow condition is the dominant factor for its appearance so reduction of flow caused by dramatic warming trend can counteract the increase of rainfall to limit the transport capacity of the bed material.

Further study on this topic under climate change context should be dedicated to: 1) comparing the modeled results under other inhomogeneous climate scenarios with different time scales (monthly, daily) to investigate the potential climate change effect on suspended sediment load and resuspension; 2) bringing in other local level anthropogenic impact projections (land use change, water use change etc.) to investigate these relative impacts. Moreover, after comprehensive improvement of the GWLF/WASP model and though understanding of the predicted results, impact assessments and mitigation strategies can be developed in the future.

References

Alley, W.M., 1981. Estimation of impervious-area washoff parameters. *Water Resources Research, 17(4)*, pp.1161-66.

Ambrose, R.B., 2009. *WASP7 stream transport model theory and user's guide*. U.S. EPA Office of Research and Development.

Amy, G., Pitt, R., Singh, R. & Bradford, W.L., 1974. *Water quality management planning for urban runoff*. EPA-440/9-75-004. U.S. Environmental Protection Agency, Washington DC.

Asselman, N.E.M., Middelkoop, H. & Dijk, P.M.v., 2003. The impact of changes in climate and land use on soil erosion, transport and deposition of suspended sediment in the River Rhine. *Hydrological Processes 17*, pp.3225–44.

Barsugli, J.J., Vogel, J.M., Kaatz, L. & Smith, J.B., 2012. Two Faces of Uncertainty: Climate Science and Water Utility Planning Methods. *Journal of Water Resources Planning and Management*, pp.389-95.

Bloesch, J., 1994. A review of methods used to measure sediment resuspension. *Hydrobiologia 284*, pp.13-18.

Brekke, L., 2013. *Errata for "Downscaled CMIP3 and CMIP5 Climate and Hydrology Projections: Release of Downscaled CMIP5 Climate Projections, Comparison with preceding Information, and Summary of User Needs"*. [Online].

Brekke, L., Thrasher, B.L., Maurer, E.P. & Pruitt, T., 2013. *Downscaled CMIP3 and CMIP5 Climate Projections*.

Brownlie, W.R., 1981. *Prediction of flow depth and sediment discharge in open channels, Report No. KH-R-43A*. Pasadena, CA: W. M. Keck Laboratory of Hydraulics and Water Resources, California Institute of Technology.

Chapra, S.C., 2008. *Surface Water-Quality Modeling*. Waveland Press, Inc.

Chien, N. & Wan, Z., 1999. *Mechanics of Sediment Transport*. Reston, VA: ASCE Press.

Einstein, H.A., 1950. *The bed load function for sediment transportation in open channels. Technical Bulletin 1026*. Washington, D.C.: U.S. Dept. of Agric, Soil Conservation Service.

Engelund, F. & Fredsoe, J., 1976. A sediment transport model for straight alluvial channels. *Nordic Hydrol., 7(5)*, pp.293-306.

Gailani, J., Ziegler, C.K. & Lick, W., 1991. Transport of suspended solids in the lower Fox River. *Journal of Great Lakes Research 17(4)*, pp.479-94.

Garcia, M. & Parker, G., 1991. Entrainment of Bed Sediment into Suspension. *Journal of Hydraulic Engineering, 117(4)*, pp.414–35.

Gomez, B. et al., 2009. Simulating changes to the sediment transport regime of the Waipaoa River,New Zealand, driven by climate change in the twenty-first century. *Global and Planetary Change 67*, pp.153–66.

Gust, G. & Morris, M.J., 1989. Erosion Thresholds and Entrainment Rates of Undisturbed in situ Sediments. *Journal of Coastal Research*, pp.87-99.

Haith, D.A., Mandel, R. & Wu, R.S., 1992. *Generalized Watershed Loading Functions Version 2.0 User's Manual*. Cornell University, Ithaca, NY.

Hamon, W.R., 1961. Estimating potential evapotranspiration. *Proceedings of the American of Civil Engineers, Journal of the Hydraulics Division 87(HY3)*, pp.107-20.

Hancock, G.R., 2012. Modelling stream sediment concentration: An assessment of enhanced rainfall and storm frequency. *Journal of Hydrology 430-431*, pp.1-12.

Howarth, R.W., Fruci, J.R. & Sherman, D., 1991. Inputs of Sediment and Carbon to an Estuarine Ecosystem: Influence of Land Use. *Ecological Applications 1(1)*, pp.27-39.

Kim, S., Mandel, R., Nagel, A. & Schultz, C., 2007. *Anacostia Sediment Models: Version 3 TAM/WASP Water Clarity Model*. Rockville, MD: Interstate Commission on the Potomac River Basin.

Kuo, C.Y., Cave, K.A. & Loganathan, G.V., 1988. Planning of urban best management practices. *Water Resources Bulletin 24(1)*, pp.125-32.

Lee, K.Y. et al., 2000. Modeling the hydrochemistry of the Choptank River Basin using GWLF and Arc/Info: 1. Model calibration and validation. *Biogeochemistry 49*, pp.143–73.

Leggett, J., Pepper, W. & Swart, R.J., 1992. *Emissions Scenarios for the IPCC*. Cambridge University Press.

Lu, X.X., Ran, L.S. & Liu, S., 2013. Sediment loads response to climate change: A preliminary study of eight large Chinese rivers. *International Journal of Sediment Research 28*, pp.0-14.

Meric, D. et al., 2013. Model Prediction of Long-Term Reactive Core Mat Efficacy for Capping Contaminated Aquatic Sediments. *Journal of Environmental Engineering 139(4)*, pp.564–75.

Milly, P.C.D. et al., 2008. Stationarity Is Dead: Whither Water Management? *Science, 319*, pp.573-74.

Nakicenovic, N. et al., 2000. *Special Report on Emissions Scenarios (SRES)*. Cambridge University Press.

Nash, J.E. & Sutcliffe, J.V., 1970. River flow forecasting through conceptual models. Part I – A discussion of principles. *Journal of Hydrology*, pp.292-90.

NECIA, 2006. *Climate change in the U.S. Northeast: A report of the Northeast Climate Impacts Assessment*.

Nelson, E.J. & Booth, D.B., 2002. Sediment sources in an urbanizing, mixed land-use watershed. *Journal of Hydrology 264*, pp.51–68.

NRCS, 1986. *Urban Hydrology for Small Watersheds TR-55*. United State Department of Agriculture.

Ogrosky, H.O. & Mockus, V., 1964. *Hydrology of agricultural lands. In: V. T. Chow (ed.). Handbook of Applied Hydrology, Ch.21*. New York: McGraw-Hill.

Roberts, J.D., Jepsen, R.A. & James, S.C., 2003. Measurements of Sediment Erosion and Transport with the Adjustable Shear Stress Erosion and Transport Flume. *Journal of Hydraulic Engineering*, pp.862-71.

Sartor, J.D. & Boyd, G.B., 1972. *Water pollution aspects of street surface contaminants*. EPA-R2/72-081. U.S.Environmental Protection Agency, Washington DC.

Schneiderman, E.M., Pierson, D.C., Lounsbury, D.G. & Zion, M.S., 2002. Modeling the hydrochemistry of the Cannonsville watershed with Generalized Watershed Loading Functions (GWLF). *Journal of the American Water Resources Association 38(5)*, pp.1323-47.

Scott, J.C., Craig, J.A., Matthew, G.D. & Jesse, R.D., 2010. Advances in sediment transport modelling. *Journal of Hydraulic Research Vol. 48, No. 6*, pp.754–63.

Selker, J.S., Haith, D.A. & Reynolds, J.E., 1990. Calibration and testing of daily rainfall erosivity model. *Transactions of the American Society of Agricultural Engineers 33(5)*, pp.1612-18.

Smith, J.D. & McLean, S.R., 1977. Spatially averaged flow over a wavy surface. *Journal of Geophysical Research, 82(12)*, pp.1735-46.

SREX, 2012. *Special report of the intergovernmental panel on climate change: Managing the risks of extreme events and disasters to advance climate change adaptation*. Intergovernmental Panel on Climate Change.

Tabak, C.L., 2003. *Predicting sediment loads in the Aberjona River, MA*. Tufts University, Medford, MA.

Thodsen, H., Hasholt, B. & Kjærsgaard, J.H., 2008. The influence of climate change on suspended sediment transport in Danish rivers. *Hydrological Processes 22*, pp.764–74.

USEPA, 2006. *Framework for developing suspended and bedded sediments (SABS) water quality criteria*. USEPA.

USEPA, 2007. *National water quality inventory report 2002*.

van Rijn, L.C., 1984a. Sediment transport I: Bed load transport. *Journal of Hydraulic Engineering. 110(11)*, pp.1431–56.

van Rijn, L.C., 1984b. Sediment transport II: Suspended load transport. *Journal of Hydraulic Engineering, 110(11)*, pp.1431-56.

van Rijn, L.C., 1984c. Sediment transport III: Bed forms and alluvial roughness. *Journal of Hydraulic Engineering. 110(12)*, pp.1733–54.

van Rijn, L.C., 1993. *Principles of sediment transport in rivers, estuaries and coastal seas*. Aqua Publications.

Vanoni, V.A., 1975. *Sedimentation Engineering*. New York, NY: American Society of Civil Engineers.

Vuuren, D.P.v., Edmonds, J., Kainuma, M. & Riahi, K., 2011. The representative concentration pathways: an overview. *Climatic Change 109*, pp.5-31.

Wischmeier, W.H. & Smith, D.D., 1978. Predicting Rainfall Erosion Losses — A Guide to Conservation Planning. In *Agricultural Handbook*. U. S. Department of Agriculture, Washington, D.C. p.537.

Woodward, D.E., Hawkins, R. & Jiang, R., 2003. Runoff Curve Number Method: Examination of the Initial Abstraction Ratio. In *Proceedings of World Water & Environmental Resources Congress*. Philadelphia, PA, 2003.

Yang, C.T., 1996. *Sediment Transport: Theory and Practice*. New York: McGraw-Hill Book Co.

Yenilmez, F. & Aksoy, A., 2013. Comparison of phosphorus reduction alternatives in control of nutrient concentrations in Lake Uluabat (Bursa, Turkey): Partial versus full sediment dredging. *Limnologica - Ecology and Management of Inland Waters, 43(1)*, pp.1-9.

Zhang, W.T. & Rao, Y.R., 2012. Application of a eutrophication model for assessing water quality in Lake Winnipeg. *Journal of Great Lakes Research Volume 38, Supplement 3*, pp.158-73.

Appendix: GWLF/WASP Input Parameters

Land use area and curve numbers (CN)

Land Use	Area (ha)	Curve Number
Low Density Mixed	101	66
Medium Density Mixed	24	76
High Density Mixed	1087	80
Low Density Residential	110	68
Medium Density Residential	1652	69
High Density Residential	964	70
Hay/Pasture	6	68
Cropland	30	75
Forest	1372	60
Wetland	317	87
Disturbed	305	85
Turf/Golf	67	62
Open Land	165	62
Water	129	100
Total	6330	

RUSLE parameters

Land Use	K	LS	C	P
Hay/Pasture	0.046	1.074	0.03	1
Cropland	0.159	1.322	0.42	1
Forest	0.13	2.435	0.002	1
Wetland	0.054	0.1	0.01	1
Disturbed	0.033	0.759	0.08	1
Turf/Golf	0.173	0.655	0.03	1
Open Land	0.124	0.811	0.04	1

GWLF model parameters

Parameter	Value	Unit
Temperature for snow accumulation	-1	℃
Temperature for snow melt	1	° C
Available water capacity	1.375	cm
Recession coefficient	0.04	
Seepage coefficient	0	
Initial unsaturated storage	10	cm
Initial saturated storage	5	cm
Initial snow	0.5	cm
Sediment delivery ratio	0.4	

GWLF model monthly parameters

Month	Cover Coefficient (CV)	Erosion Coefficient	Growing Season
Jan	2.5	0.11	No
Feb	2.5	0.11	No
Mar	2.5	0.11	No
Apr	2.5	0.22	Yes
May	2.5	0.22	Yes
Jun	2.5	0.22	Yes
Jul	2.5	0.22	Yes
Aug	2.5	0.22	Yes
Sep	2.5	0.22	Yes
Oct	2.5	0.11	No
Nov	2.5	0.11	No
Dec	2.5	0.11	No